Supplemental Materials and Methods:

Antibodies and reagents

The following antibodies were used: anti-LYVE-1, Abcam (ab14917), immunoblot and IHC; anti-VEGF-C, Abcam (ab9546), immunoblot and IHC; VEGF-C neutralizing anti-body (pV1006R-r, Angio-Proteomie, Boston, USA); anti-luciferase, Abcam (ab21176), IHC; anti-SNAI2, Abcam (ab106077), immunoblot and IHC; anti-MMP9, Abcam (ab38898), immunoblot and IHC; anti-β-tubublin (CellSignaling Technology, #2146), immunoblot; anti-β-actin (Cell Signaling Technology, #4970), immunoblot; anti-GAPDH (Cell Signaling Technology, #5174), immunoblot; anti-E-cadherin (Cell Signaling Technology, #3195), immunofluorescence and immunoblot; anti-N-cadherin, Abcam (ab98952), immunofluorescence and immunoblot; anti-Vimentin, Abcam (ab92547), immunofluorescence and immunoblot; anti-Fibronectin, Abcam (ab2413) , immunofluorescence and immunoblot; anti-WDR5, Abcam (Ab56919) (Immunoblot, RIP and ChIP); anti-H3K4me3, Abcam (Ab8580), (immunoblot and ChIP); Anti-rabbit IgG, HRP-linked Antibody, CST(Cat #7074), Immunoblot; Anti-mouse IgG, HRP-linked Antibody, CST(Cat #7076), Immunoblot; control Mouse and Rabbit IgG, anti-RNA pol II, and anti-snRNP70 were provided in EZ-Magna RIP kit or EZ-Magna ChIP A/G kit (Millipore). TGF-β was purchased from R&D Systems (R&D Systems Inc., Minneapolis, MN, USA). DAPI (Thermo Scientific, 62247), Alexa Fluor™ 555 Phalloidin (Invitrogen™).

Microarray and data analysis

For microarray analysis, RNA purity and integrity was analyzed by Agilent Bioanalyzer 2100 (Agilent). Qualified total RNA was further purified by RNeasy mini kit (QIAGEN) and RNase-free DNase set (QIAGEN). Total RNA was then amplified and labeled by Low Input Quick Amp Labeling Kit, One-Color (Agilent), following the manufacturer's instructions. Labeled cRNA were purified by RNeasy mini kit (QIAGEN). Each Slide was hybridized with 600ng Cy3-labeled cRNA using Gene Expression Hybridization Kit (Agilent) in Hybridization Oven (Agilent), according to the manufacturer's instructions. After 17 hours hybridization, slides were washed in staining dishes (Thermo Shandon) with Gene Expression Wash Buffer Kit (Agilent), following the manufacturer's instructions. Slides were scanned by Agilent Microarray Scanner (Agilent) with default settings, Dye channel: Green, Scan resolution=3 μm, 20 bit. Data were extracted with Feature Extraction software 10.7 (Agilent). Raw data were normalized by Quantile algorithm, Gene Spring Software 11.0 (Agilent).

Cell culture and transfection

Human bladder cancer cell lines UMUC-3, HT-1376, 5637, TCCSUP, T24, J82 and RT4, and immortalized normal urothelial cell line SV-HUC-1 were purchased from American Type Culture Collection (ATCC, USA). Human bladder cancer cell line EJ was from Institute of Urology, Peking University as a gift. 5637 cells were maintained in RPMI-1640. UMUC-3, HT-1376, T24, J82, EJ, RT4 and TCCSUP were cultured in Dulbecco's modified eagle's medium (DMEM) (Hyclone), SV-HUC-1 were cultured in F-12K medium (Hyclone). All culture medium were supplemented with 10% fetal bovine serum (FBS), 100 U/ml penicillin, and 100 μg/ml streptomycin

(HyClone, Thermo, USA). All cells were cultured in a humidified air atmosphere incubator with 5% CO2 at 37°C. RNA interference (RNAi) was performed using RNAiMAX (Life Technologies) following manufacturer's instructions. All siRNA oligos were purchased from GenePharma (Shanghai).

RNA isolation and Quantitative reverse transcription PCR (RT-qPCR)

Total RNA from cells was isolated using Trizol reagent (Life techologies) and purified with GeneJET RNA purification kit (Thermo) and RNase-free DNase set (QIAGEN) following manufacturer's instructions.RNA electrophoresis was conducted to inspect RNA integration. Reverse Transcription was performed using M-MLV Reverse Transcriptase (Life technologies) and quantitative PCR was performed with SYBR green master mix (Roche). Relative expression values were calculated (ΔΔCT method) using GAPDH as a normalizer.

Lentivirus transduction.

To establish stable overexpression and knockdown cell lines, full length of BLACAT2 or shRNA sequences that specifically target BLACAT2 or VEGF-C were cloned into Vectors of pCDH-CMV-MCS-EF1-Puro (with or without luciferase) or pLKO.1-Puro (with or without luciferase) and bidirectional sequenced, respectively. Sequences of all shRNAs were listed in Supplemental Table 4. Viral particles were obtained through Lipofectamine 2000 (Life Technologies, USA) transfection in HEK293T packaging cell lines, and with VSVG, RSV-Revpackaging plasmids. Viral supernatants were harvested after 48h of transfection. The supernatant then was clarified by centrifugation (5,000 × g for 5 min at room temperature), passed through a

polyvinylidene fluoride filter (pore size, 0.45 μm) and the titer was dectected. Cells were infected by lentivirus with the presence of polybrene (Sigma-Aldrich) and selected by puromycin (Sigma-Aldrich) for 2 weeks to obtain stable expression cell lines.

Rapid amplification of cDNA ends (RACE).

5’ and 3’-RACE analyses were performed using the GeneRacer kit (Life Technologies, Cat. No. L1500-01) according to manufacturer’s instructions. The sequences of BLACAT2 specific primers used in nested PCR of RACE assay are shown in Supplemental Table 5. PCR products were cloned into pCR4-TOPO using the TOPO TA cloning kit (Life Technologies). At least 10 resulting clones were bidirectional sequenced.

Nuclear Fractionation

Nuclear Fractionation has been described in detail previously(1). Briefly, For nuclear fractionation,1×10^7cells were harvested, washed with PBS and resuspended in 1ml of RNase-free PBS, 1ml of buffer C1 (1.28 M Sucrose, 40 mM Tris, pH 7.5, 20 mM $MgCl_2$, 4% Triton X-100) and 3mlof RNase-free water, and incubated for 15 min on ice. Then cells were centrifuged for 15 min at 2500 rpm, the supernatant was discarded and the nuclear pellet was kept for RNA extraction.

Cell motility and invasion assay

The migration of cells was evaluated using transwell chamber (BD Biosciences, MA, USA) according to the manufacture's protocol. Cells were subjected to 24 h of serum deprivation and plated into chambers in serum-free medium. Bottom wells

were filled with complete medium. Cells were allowed to migrate for 24 h. The migrated cells from random fields were chosen then counted, using the computer-based microscopy imaging system. For the invasion assay, the same procedures except that the cells were plated into 24-well matrigel-coated transwell plates (BD Biosciences, MA, USA).

Immunoblotting analysis

Cells were lysed in RIPA buffer (Pierce) supplemented with 1 mM protease inhibitor cocktail (Roche). The cell lysates were sonicated and centrifuged to remove debris, and equal amounts of protein were separated on polyacrylamide gels and incubated with antibodies. The signal was detected by enhanced chemiluminescence (Millipore).

Immunofluorescence assay and cytoskeleton staining

Cells were cultured on coverslips and fixed with 4% paraformaldehyde and permeabilized with 0.1% Triton X-100 in PBS for 5 minutes at room temperature. After blocking with 1% BSA in PBS, cells were incubated with specific primary antibodies for 60 min or TRITC-conjugated phalloidin (Sigma-Aldrich, USA) for 30 min at room temperature. For immunofluorescence, cells were further washed with PBS and incubated with Goat anti-Mouse IgG (H+L) Cross-Adsorbed Secondary Antibody, Alexa Fluor 488 (Thermo Scientific, Cat #A-11001), Goat anti-Rabbit IgG (H+L) Cross-Adsorbed Secondary Antibody, Alexa Fluor 488 (Thermo Scientific, Cat #A-11008) or Goat anti-Rabbit IgG (H+L) Cross-Adsorbed Secondary Antibody, Alexa Fluor 633 (Thermo Scientific, Cat #A-21070). Cells were counterstained with

DAPI(Thermo Scientific, Cat #62248), mounted and observed withZeiss confocal microscope (Zeiss 710).

Human lymphatic endothelial cell tube formation assay.

Serum-free media obtained from 24-hour-cultured bladder cancer cells was concentrated 10-fold using ultrafiltration spin columns (Millipore, Billerica MA). HLECs were then seeded into 6-well plates (pre-coated with Matrigel) that contained concentrated media and incubated for 8hours. The resulting lymphatic tubes were photographed using an inverted microscopeand quantified by measuring the number and area of the completed tubule structures.

Wound healing assay and 3D culture.

For wound healing assay, cells were seeded at 4×10^4 cells/cm^2 and were grown to 90% confluency. A straight scratch was made with a 200 µL pipette tip and the plate was incubated at 37°C in serum-free medium after 3 washes with PBS. The migration of cells into the wound area was analyzed and photographed using an inverted microscope.

For the 3D cultures, cells were mixed with collagen I matrix and seeded into 6-well plates. Cultures were maintained in a 37°C humidified incubator ventilated with 5% CO_2 for up to 96 h. At designated time-points, plates were washed with PBS, fixed for 45 min with 3.7% formaldehyde at room temperature and photographed with a microscope.

Subcutaneous tumorigenicity and tail vein injection assay

All animal procedures involving animals were approved by the Institute Animal

Care and Use Committee of Sun Yat-sen University. Combined immunocompromised NOD/SCID mice at the age of 4-5 weeks old were purchased from Beijing Vital River Laboratory Animal Technology Corporation and 8 mice were used in each group. For subcutaneous tumorigenicity assay, 1×10^6 cells transduced with BLACAT2-luciferase, vector-luciferase, shBLACAT2-luciferase or shControl-luciferase in 200 μl phosphate buffer saline were inoculated subcutaneously. For tail vein injection assay, 1×10^6 cells were injected into tail vein of each mice. Mice were observed weekly for signs of illness. Lung metastasis were monitored and quantified with a bioluminescence imaging system (PerkinElmer, IVIS Spectrum Imaging System) after 4 weeks post-injection. The tumors and lungs were excised and fixed in formalin overnight and embedded in paraffin, from which sections were stained with hematoxylin and eosin and/or anti-luciferase by pathologists. RT-PCR and in situ hybridization were used to confirm BLACAT2 expression at the end of the experiment. For bioluminescence imaging, mice received luciferin (300 mg/kg, 10 min before imaging) and were anesthetized with 3% isoflurane, imaged in an IVIS spectrum imaging system.

Serial deletion analysis and site-directed mutagenesis.

Serial 3' nested PCR primers and common 5' primers, or serial 5' nested PCR primers and common 3' primers were used to amplify serial deletion fragments of BLACAT2 and the resulting fragments were inserted into pcDNA3.0 for *in vitro* transcription in the RNA pull down assay. BLACAT2 was mutated using the Quick Change Site-directed Mutagenesis Kit (Stratagene, La Jolla, CA, USA) according to

the manufacturer's instructions. Primers for site-directed mutagenesis are listed in Supplemental Table 5.

Next-generation sequencing.

Total RNA was extracted using the TRIzol reagent (Invitrogen, USA) and incubated for 1 hour at 37°C with 10 units of DNase I (TaKaRa, Dalian, China) to eliminate genomic DNA. RNA quality was analyzed using a BioAnalyzer 2100 (Agilent Technology, Santa Clara, CA). Purified total RNA (3μg) was used to deplete ribosomal RNA using Ribo-Zero rRNA Removal Kits (MRZMB126,Epicentre). Poly(A)+ RNA was purified using oligo(dT) magnetic beads and fragmented into short sequences. The library was prepared using the TruSeq Stranded mRNA LT Sample Prep Kit (Cat. No.15032612, Illumina) according to the manufacturer's instructions. Each library was sequenced on an Illumina HiSeq2500 in 125PE mode (Illumina, San Diego, CA, USA).

ELISA-based quantification of secreted VEGF-C.

The cell culture supernatant was collected, and the secreted VEGF-C was quantified using the Human VEGF-C Quantikine ELISA Kit (Cat. No. DVEC00, R&D) according to the manufacturer's instructions.

RNA pull down assay and Mass spectrometry.

Full-length BLACAT2 and antisense BLACAT2 sequences were prepared by *in vitro* transcription using TranscriptAid T7 High Yield Transcription Kit (Thermo Scientific) and treated with RNase-free DNase I and purified with GeneJET RNA purification kit (Thermo Scientific). RNA pull down assay was performed with

Magnetic RNA-Protein Pull-Down Kit (Thermo Scientific) according to manufacturer's instructions. Nuclear extracts were prepared with NE-PER Nuclear Protein Extraction Kit (Thermo Scientific). Three micrograms of biotin-labeled RNA and 1 mg of nuclear extract were used in each pull down assay. The retrieved protein was separated in polyacrylamide gels and detected with silver stain kit (Thermo) or standard immunoblot technique. For RNA pull down assay with *in vitro* synthesized protein, full length of ORF fragment of a specific gene was inserted into pcDNA3.0 and was *in vitro* transcribed and translated with 1-Step Human Coupled In Vitro Expression Kit (Thermo) following standard protocols.

Circular dichroism (CD) spectroscopy

CD-spectra were performed on a Chirascan (Applied Photophysics Limited) as previously described(2). Specifically, CD-spectra were recorded on BLACAT2ssRNA TFO (2.2μM) and the three different dsDNA TTS oligos (corresponding to the VEGF-C,SNAI2, and MMP9promoter sequences predicted to be associated with BLACAT2, 2.2 μM each) separately as well as on a1:1 mix of the two (2.2 μM TFO and 2.2 μM TTS) in 1× triplex forming buffer(10mM Tris pH 7.5, 25mM NaCl and 10mM $MgCl_2$). For comparison, sample with a control ssRNA was included (negative control). The mixed samples or individual RNA and dsDNAs were equilibrated approximately 1h at 30°C. The measurements were performed at room temperature in a 1 mm cuvette using 200 μL solutions and kept at room temperature before the measurement.

Bioinformatic analysis

LongTarget was used to predict Triplex forming oligos (TFOs) and Triplex target sites (TTS)(3).

References

1. He W, et al. linc-UBC1 physically associates with polycomb repressive complex 2 (PRC2) and acts as a negative prognostic factor for lymph node metastasis and survival in bladder cancer. *BBA-Mol Basis Dis.* 2013;1832(10):1528-1537.
2. Mondal T, et al. MEG3 long noncoding RNA regulates the TGF-β pathway genes through formation of RNA–DNA triplex structures. *Nat Commun.* 2015;6:7743.
3. He S, et al. LongTarget: a tool to predict lncRNA DNA-binding motifs and binding sites via Hoogsteen base-pairing analysis. *Bioinformatics.* 2015;31(2):178-186.

Supplemental Table 1. Patient characteristics for microarray analysis.

Patient	Gender	Age(yrs)	TNM stage	Pathological grade
BCa1	Male	59	T2aN0M0	III
BCa2	Male	66	T3aN1M0	III
BCa3	Male	68	T2aN2M0	III

Supplemental Table 2. Characteristics of bladder cancer patients.

Characteristic	Patient frequency	BLACAT2		Pearson Chi-square	*p* value
		Low	High		
Total	140	47	93		
Gender					
Male	108 (77.1%)	36	72	0.012	0.913
Female	32 (22.9%)	11	21		
Age					
<60	58 (41.4%)	17	41	0.806	0.369
≥60	82 (58.6%)	30	52		
Tumor stage					
T1	37 (26.4%)	13	24	0.06	0.814
T2-4	103 (73.6%)	34	69		
Tumor grade					
Low	28 (28.6%)	19	21	4.872	0.027
High	112 (71.4%)	28	72		
L.N. status					
N(-)	99 (70.7%)	39	60	5.139	0.023
N(+)	41 (29.3%)	8	33		

Supplemental Table 3. Inhibition of VEGF-C signaling reduces BLACAT2-induced popliteal lymph node metastasis *in vivo*

UMUC-3 xenograft	No. total LNs	No. metastatic LNs	Metastatic ratio (%)
Vector+shControl	12	5	41.6
Vector+shVEGF-C	12	1	8.3
BLACAT2+shControl	12	12	100
BLACAT2+ shVEGF-C	12	1	8.3
Vector+IgG	12	4	33.3
Vector+anti-VEGF-C	12	0	0
BLACAT2+IgG	12	12	100
BLACAT2+ anti-VEGF-C	12	0	0

Supplemental Table 4. Sequences of siRNA oligos and shRNAs used in this study.

siRNAs	Sense	Antisense
shControl	5’-CCGGCAACAAGATGAAGAGCACCAACTCGAGTTGGTGCTCTTCATCTTGTTGTTTTTG-3’	5’-CAAAAACAACAAGATGAAGAGCACCAACTCGAGTTGGTGCTCTTCATCTTGTTGCCGG-3’
shBLACAT2 #1	5’-CCGGTAGACCAAGACCTGGAATTAACTCGAGTTAATTCCAGGTCTTGGTCTATTTTTG-3’	5’-CAAAAATAGACCAAGACCTGGAATTAACTCGAGTTAATTCCAGGTCTTGGTCTACCGG-3’
shBLACAT2 #2	5’-CCGGCTCCTGCAGTTTCTGAACACTCTCGAGAGTGTTCAGAAACTGCAGGAGTTTTTG-3’	5’-CAAAAACTCCTGCAGTTTCTGAACACTCTCGAGAGTGTTCAGAAACTGCAGGAGCCGG-3’
shBLACAT2 #3	5’-CCGGCAGTGTCCTCTTGCTATTGAACTCGAGTTCAATAGCAAGAGGACACTGTTTTTG-3’	5’-CAAAAACAGTGTCCTCTTGCTATTGAACTCGAGTTCAATAGCAAGAGGACACTGCCGG-3’
shVEGF-C#1	5’-CCGGCTACCTCAGCAAGACGTTATTCTCGAGAATAACGTCTTGCTGAGGTAGTTTTTG-3’	5’-CAAAAACTACCTCAGCAAGACGTTATTCTCGAGAATAACGTCTTGCTGAGGTAGCCGG-3’
shVEGF-C#2	5’-CCGGGGCCAACCGAGAATTTGATGACTCGAGTCATCAAATTCTCGGTTGGCCTTTTTG-3’	5’-CAAAAAGGCCAACCGAGAATTTGATGACTCGAGTCATCAAATTCTCGGTTGGCCCCGG-3’
shSNAI2	5’-CGGGAGTGACGCAATCAATGTTTACTCGAGTAAACATTGATTGCGTCACTCTTTTTG -3’	5’-AATTCAAAAAGAGTGACGCAATCAATGTTTACTCGAGTAAACATTGATTGCGTCACTC-3’
siControl	5’-AGCUGACCCUGAAGUUCAU dTdT-3’	5’-AUGAACUUCAGGGUCAGCU dTdT-3’
siWDR5#1	5’-CGAUGUAGCCUGGUCGUCA dTdT-3’	5’-UGACGACCAGGCUACAUCG dTdT-3’
siWDR5#2	5’-CAUUUCUUGCCAAUUCUAAdTdT-3’	5’-UUAGAAUUGGCAAGAAAUG dTdT-3’

Supplemental Table 5. Primers used in this study.

Primers	Up stream	Down stream	Application
BLACAT2	5’-GAGAGGGATCCACTCATCCA-3’	5’-TGGAAACAAAGGCAGAGCTT-3’	qRT-PCR
BLACAT2 5’-RACE	Universal primer included in GeneRacer kit	5’-CTCTGCCGCCTGGGTTCAAGCGATT-3	5’-RACE(Nested PCR, outer)
BLACAT2 5’-RACE	Universal primer included in GeneRacer kit	5’-GCCTGAGCTTCTTCCTGTAGACTGT-3’	5’-RACE(Nested PCR, inner)
BLACAT2 3’-RACE	5’-AGCCAGAGAGGAGGAGAAGCAATCA-3’	Universal primer included in GeneRacer kit	3’-RACE (Nested PCR, outer)
BLACAT2 3’-RACE	5’-GAGAGGGATCCACTCATCCA-3’	Universal primer included in GeneRacer kit	3’-RACE (Nested PCR, inner)
GAPDH	5’-TGGTGAAGACGCCAGTGGA-3’	5’-GCACCGTCAAGGCTGAGAAC-3’	qRT-PCR

HOTTIP	5’-CCTAAAGCCACGCTTCTTTG-3’	5’-TGCAGGCTGGAGATCCTACT-3’	qRT-PCR
BLACAT2 primer A（1-200）	5’-CCTGCTGCATTGTGAAGAAAC-3’	5’-TCTGATGTGTTAATTCCAGGTCT-3’	qRT-PCR
BLACAT2 primer B	5’- GGACTCTTGTGACCAGGACA-3’	5’- TACCTGGCGTCTGTGTAGTG-3’	qRT-PCR
WDR5	5’-GGAATATCCGATGTAGCCTGGT-3’	5’-GGGGATTGAAGTTGCAGCAAA-3’	qRT-PCR
U1	5’-GGGAGATACCATGATCACGAAGGT-3’	5’-CCACAAATTATGCAGTCGAGTTTCCC-3’	qRT-PCR
VEGF-C	5’-GGCTGGCAACATAACAGAGAA-3’	5’-CCCCACATCTATACACACCTCC-3’	mRNA qRT-PCR
SNAI2	5’-GCGAACTGGACACACATACA-3’	5’-AAGAGGAGAGAGGCCATTGG-3’	mRNA qRT-PCR
MMP9	5’-GGGACGCAGACATCGTCATC-3’	5’-TCGTCATCGTCGAAATGGGC-3’	mRNA qRT-PCR
U6	5’-CGCTTCGGCAGCACATATACTA-3’	5’-TCACGAATTTGCGTGTCATCCT-3’	RNA qRT-PCR
p53	5’-GAGGTTGGCTCTGACTGTACC-3’	5’-TCCGTCCCAGTAGATTACCAC-3’	mRNA qRT-PCR
p21	5’-TGTCCGTCAGAACCCATGC-3’	5’-AAAGTCGAAGTTCCATCGCTC-3’	mRNA qRT-PCR
VEGF-C	5’-GCACTGCATCCTGAGAACTG-3’	5’-GCCCTGCTCAAAGTTTGGAA-3’	ChIP-qPCR
SNAI2	5’-CTGGTTCAAAATGGGCTGTT-3’	5’-GCTGCACCACATCTGGAAG-3’	ChIP-qPCR
MMP9	5’-AGCCTGGGTGATAGAGTGAT-3’	5’-TTCTTCCTAGCCAGCCGG-3’	ChIP-qPCR
β-actin	5’-CAGCAGTCGGTTGGAGCGAGCAT-3’	5’-GGACTTCCTGTAACAACGCATCTC-3’	ChIP-qPCR
VEGF-C-1	5’-CCCAGTGAGAGATCCCGAAA-3’	5’-CGAGCATTTCCCGACCAAAA-3’	ChIRP
VEGF-C-2	5’-CGGCTCCTCTCACTTCGGGGA-3’	5’-ATTCGGAGCCCGCGAGGTGA-3’	ChIRP
VEGF-C-3	5’-GAGGGAAACGGGGAGCTCCA-3’	5’-CTTATGTGAGAGAAAGCGGCCGA-3’	ChIRP
VEGF-C-4	5’-TTCCAAACTTTGAGCAGGGC-3’	5’-GGCTTTAGAGGTGATGCGAC-3’	ChIRP
VEGF-C-5	5’-TGGGGAAATGCAGTCACTTT-3’	5’-TGACAGGTGAAGAGAAGGGC-3’	ChIRP
VEGF-C-6	5’-AGATTGGGAGTGAAAGGCAG-3’	5’-GGGGTTTCCGTTGGGCTG-3’	ChIRP
VEGF-C-7	5’-GAAGGACTCAGTTGTGGAAGT-3’	5’-CACCCATAATTTACTTGAAGGCTTA-3’	ChIRP
VEGF-C-8	5’-AACACTGTGATTTGGCTGCC-3’	5’-GGCTCGGTACTTAGTGCTGT-3’	ChIRP
VEGF-C- 9	5’-AAATCCTACCCCAGTCTGCC-3’	5’-CGGTCCATGATCTAGCCTGT-3’	ChIRP
SNAI2-1	5’-AGCATTTCAACGCCTCCAAA-3’	5’-GGAAAACAGTTGAATCTTTGGCT-3’	ChIRP
SNAI2-2	5’-ACAGCCCATTTTGAACCAGA-3’	5’-GAAGTCACCCGGCTCCTTTA -3’	ChIRP
SNAI2-3	5’-TCCAGGCCAGAGTCCCAGGA-3’	5’-GTGGCATCTGGAGAGGTTTGCC-3’	ChIRP
SNAI2-4	5’-TGACAGTTACCTCTTGCCCC-3’	5’-CCGCGTGCAAATTAAGTACTC-3’	ChIRP
SNAI2-5	5’-GGAACCACCGGACATTCTCT-3’	5’-GGAACCACCGGACATTCTCT-3’	ChIRP

SNAI2-6	5’-TCATGTGAATTTGTTCTTTCC -3’	5’-CTGCAAAAACACCTTTATTTTG -3’	ChIRP
SNAI2-7	5’-GCTCTCATAAACCCAGGTGC-3’	5’-TGCTAATGGAACTGTACTTGCA-3’	ChIRP
SNAI2-8	5’-GGGGCTGGGCTGGATTATG-3’	5’-TCCTTGTTTCACTCTACACAGTC-3’	ChIRP
SNAI2-9	5’-GCACCTGTTTCGTCTGACTC-3’	5’-CTACTGTGAGGAGAGGATGGG-3’	ChIRP
MMP9-1	5’-GCTTTAGGGGTGTGTTGGTG-3’	5’-ATGCTTACCCCAGAACCCTC-3’	ChIRP
MMP9-2	5’-GCCCTTTCTCATGCTGGTG-3’	5’-GTGAGGGCAGAGGTGTCT-3’	ChIRP
MMP9-3	5’-TCAGAAAGAAGTCTCAGGGAGT-3’	5’-GGGGTAGGGTTTTGCAAACT-3’	ChIRP
MMP9-4	5’-TTCCAAACTTTGAGCAGGGC-3’	5’-GGCTTTAGAGGTGATGCGAC-3’	ChIRP
MMP9-5	5’-AAGCAATCCTCCCACCTCG-3’	5’-ACTGTAGGTTGTAAGTCCGCA-3’	ChIRP
MMP9-6	5’-TCCTAAGCTGACAAAGGGGA-3’	5’-CGAGACCCTGCCAAAAGAC-3’	ChIRP
MMP9-7	5’-AGGGCTTTGAAGAAGGTGAAT-3’	5’-CCTTTCAGTTCTCCAGCCCT-3’	ChIRP
MMP9-8	5’-CGTAGTGAAACCCCATCTCTACT-3’	5’-GGGGTGTAGTATCACTCTGTCA-3’	ChIRP
MMP9-9	5’-GGACTTCGTGACTGCAAAGC-3’	5’-AAGCTGTATTTAAAGGGCCTACT-3’	ChIRP
Mut-BLACAT2(33-66)-F	5’-CTGCTGCATTGTGAAGAAACAGGTAGGTACGCACACTCGCACAGGACTATGCAGAGGCCTCCCCAGCC-3’		Site-directed mutagenesis
Mut-BLACAT2(33-66)-R	5’-TGCATAGTCCTGTGCGAGTGTGCGTACCTACCTGTTTCTTCACAATGCAGCAGGAGAGAGAGAGAG-3’		Site-directed mutagenesis

Supplemental Table 6. Probes used in In situ hybridization (ISH) and Chromatin isolation by RNA purification (ChIRP).

Probe name	Sequences	Label	Application
Scramble	5’-GTGTAACACGTCTATACGCCCA-3’	5’-DIG labeled and 3’-DIG labeled	ISH
U6	5’-CACGAATTTGCGTGTCATCCTT-3’	5’-DIG labeled and 3’-DIG labeled	ISH
BLACAT2	5’-TGTTGATGATGGATGAGTGGAT-3’	5’-DIG labeled and 3’-DIG labeled	ISH
ACTB	5’-CTCATTGTAGAAGGTGGGTGCCA-3’	5’-DIG labeled and 3’-DIG labeled	ISH
Odds-1	5’- CTCATAGAATCTTCTGATGTGT-3’	no	ChIRP
Odds-2	5’-TCTGTGTAGTGTTCAGAAACTG -3’	no	ChIRP
Odds-3	5’-AAGCCTTTTCAATAGCAAGAGG -3’	no	ChIRP
Odds-4	5’-CTTATCAGTGGACTCATCTTTG-3’	no	ChIRP
Even-1	5’-CTCAGTTGTTCTCAAAATCGTG -3’	no	ChIRP

Even-2	5’-CATTAGAGAGAGCTTAATCTGC -3’	no	ChIRP
Even-3	5’-GGCAATGATTAAGCAGTCAGAA-3’	no	ChIRP
Even-4	5’-GTCTTAACCTGCAATGATAACT-3’	no	ChIRP

Supplemental Figures and legends:

Supplemental Figure 1. BLACAT2 expression is overexpressed in high grade, metastatic bladder cancer and negatively correlates with prognosis. (**A**) Comparison of BLACAT2 expression in primary human bladder cancer samples and paired metastatic LNs. The nonparametric Mann-Whitney U test was used to compare the expression levels of the two groups. (**B**) QRT-PCR analysis of BLACAT2 expression in the 140-case cohort of freshly collected human bladder cancer samples with or without LN metastasis. (**C**) BLACAT2 expression in bladder cancer and normal urothelium from TCGA database. The nonparametric Mann-Whitney U test was used to compare the expression levels of the two groups. (**D**) Negative correlation between BLACAT2 expression and survival in the patient cohort referred to in Figure 1B. The Kaplan-Meier method was used to estimate survival for the 2 groups. The median BLACAT2 expression was used as a cutoff value.

Supplemental Figure 2. BLACAT2 is overexpressed in multiple types of human cancer. (**A-G**) Data from the GEO and TCGA databases were analyzed in different types of cancers as indicated, including bladder cancer. The Mann-Whitney U test was used to compare differences between the two groups. Means with95% confidence intervalsare shown. (**H**) The GEO data showed that BLACAT2 overexpression correlates with a poor prognosis of glioma.

Supplemental Figure 3. BLACAT2 is localized in the nucleus in bladder cancer. (**A**) Schematic visualization of the chromosomal location of BLACAT2, its neighboring protein-coding genes and the alternative splicing isoforms of BLACAT2 determined using the RACE assay. (**B**) Representative image of agarose gel electrophoresis and bidirectional sequencing of the 5’-RACE products of BLACAT2 showing the cap sequence and 5’-terminal sequence of BLACAT2. At least 10 E.coli

clones were sequenced. (**C**) Representative image of agarose gel electrophoresis and bidirectional sequencing of the 3'-RACE products of BLACAT2 showing the cap sequence and 3'-terminal sequence of BLACAT2. At least 10 E.coli clones were sequenced. (**D**) Representative images of the in situ hybridization (ISH) of BLACAT2 expression (blue) in the paraffin-embedded normal urothelium (n=20) and tumor sections of bladder cancer with or without LN metastasis (n=140). Samples were counterstained with nuclear fast red. The nuclear localized U6 probe was used as the technical positive control. (**E, F**) ISH analysis (E) and nuclear fractionation assay (F) showing that BLACAT2 preferentially localizes to the nucleus. Scramble probe served as the negative control, and β-actin served as the positive control in the cytoplasm.

Supplemental Figure 4. Efficiencies of BLACAT2 overexpression and knockdown and representative image of popliteal LN metastasis model. (**A, B**) Quantitative RT-PCR analysis of BLACAT2 expression levels in BLACAT2-transduced, BLACAT2-silenced and control cells as indicated. The error bars indicate the standard deviation of the mean. Statistical significance was assessed using two-tailed Student's t-tests (A) and one-way analyses of variance (ANOVA) followed by Dunnett's tests for multiple comparisons (B). ** $p<0.01$. (**C**) Representative image of the nude mouse model of popliteal LN metastasis. UM-UC-3 cells transduced with according vectors were injected into the footpads of nude mice, and popliteal LNs were enucleated and analyzed until the mice died or after 60 days.

Supplemental Figure 5. BLACAT2 overexpression promotes LN metastasis of HT-1376 cells in vivo. (**A**) Representative images of enucleated popliteal LNs (left panel) after the overexpression or silencing of BLACAT2 as indicated are shown, and a histogram analysis of the LN volume is included (right panel). Scale bar: 5 mm.

Error bars indicate the standard deviation of the mean, n=12. * $p<0.05$, ** $p<0.01$, Student's t-test. (**B**) Representative images of popliteal LNs analyzed by immunohistochemistry (IHC) staining with anti-luciferase antibody (n=12 per group). Scale bars: black, 500 μm; red, 50 μm.

Supplemental Figure 6. BLACAT2 overexpression promotes LN metastasis and correlates with a poor prognosis in vivo. (**A**) The ratios of metastatic to total enucleated popliteal LNs for the indicated group. (**B**) Kaplan-Meier survival analysis of the mice (n=12 per group) that were inoculated with the indicated cells. The Kaplan-Meier (Mantel-Cox) test was used to evaluate the significant difference of the survival curves.

Supplemental Figure 7. BLACAT2 overexpression promotes lung metastasis. (**A**) Histogram analysis of the volumn of footpad tumor. UM-UC-3 cells were transduced with vectors as indicated. The error bars represent standard deviation of the mean, n=12, ** $p<0.01$, Student's t test. (**B**) Lung metastasis was confirmed by hematoxylin and eosin staining. Scale bars: black, 200 μm; red, 50 μm.

Supplemental Figure 8. BLACAT2 overexpression promotes HLECs migration. (**A, B**) Representative images (left panel) and histogram quantification (right panel) of Transwell migration assay with HLECs cultured with conditioned medium derived from bladder cancer cells after overexpression or knockdown of BLACAT2. Scale bars: 200 μm. All experiments in vitro were performed with at least three biological replicates. The error bars indicate the standard deviation of the mean. Statistical significance was assessed using two-tailed Student's t-tests (A) and one-way analyses of variance (ANOVA) followed by Dunnett's tests for multiple comparisons (B). ** $p<0.01$.

Supplemental Figure 9. BLACAT2 overexpression promotes bladder cancer cell migration. (**A, B**) Representative images of the wound healing assay using bladder cancer cells (left panels) showing cell motility after ectopic expression (A) or knockdown (B) of BLACAT2 at the indicated time are shown, and a histogram analysis of the cell migration distance is provided (right panels). (**C, D**) Representative images of transwell migration assays of bladder cancer cells (left panels) showing cell motility after ectopic expression (C) or knockdown (D) of BLACAT2 are shown, and a histogram analysis of the migrated cell counts is provided (right panels). Error bars represent the standard deviation of the mean of three independent experiments. Scale bars: 200 μm. Statistical significance was assessed using two-tailed Student's t-tests (C) and one-way analyses of variance (ANOVA) followed by Dunnett's tests for multiple comparisons (A, B and D). ** $p<0.01$.

Supplemental Figure 10. BLACAT2 overexpression promotes invasiveness of bladder cancer cells. (**A, B**) Representative images (left panel) and histogram quantification (right panel) of the Matrigel invasion assay after BLACAT2 overexpression (A) and depletion (B), compared with the controls. Scale bars: 200 μm. (**C**) Representative images of the 3D culture of UM-UC-3 cells embedded in Matrigel for 5 days. Cells were treated as indicated. Scale bars: 50 μm. All experiments in vitro were performed with at least three biological replicates. The error bars indicate the standard deviation of the mean. Statistical significance was assessed using two-tailed Student's t-tests (A) and one-way analyses of variance (ANOVA) followed by Dunnett's tests for multiple comparisons (B). ** $p<0.01$.

Supplemental Figure 11. BLACAT2 overexpression promotes EMT of bladder cancer cells. (**A, B**) Histogram analysis of the mRNA expression levels of EMT

molecular biomarkers quantified by qRT-PCR after ectopic expression (A) or knockdown (B) of BLACAT2. Error bars represent the standard deviation of the mean of three independent experiments. Statistical significance was assessed using two-tailed Student's t-tests (A) and one-way analyses of variance (ANOVA) followed by Dunnett's tests for multiple comparisons (B). ** $p<0.01$. (**C**) Immunofluorescence showing E-cadherin expression and phalloidin staining showing cytoskeletal remodeling after BLACAT2 overexpression. (**D, E**) Immunofluorescence showing that depletion of BLACAT2 reverses TGF-β-induced up-regulation of the mesenchymal markers N-cadherin, vimentin (D) and fibronectin (E) and cytoskeletal remodeling as determined byphalloidin staining. (**F**) Western blot analysis of E-cadherin, N-cadherin and vimentin expression after overexpression or silencing of BLACAT2. TGF-β was used to induce EMT in5637 and HT-1376 epithelial cells.

Supplemental Figure 12. BLACAT2 depletion partially reverses themesenchymal phenotype of UM-UC-3 bladder cancer cells at baseline. (**A**) Histogram analysis of the mRNA expression levels of EMT molecular biomarkers quantified by qRT-PCR after depletion of BLACAT2. Error bars represent the standard deviation of the mean of three independent experiments. Statistical significance was assessed using one-way analyses of variance (ANOVA) followed by Dunnett's tests for multiple comparisons (B). ** $p<0.01$. (**B**) Western blot analysis of E-cadherin, N-cadherin, fibronectin and vimentin expression after silencing of BLACAT2.

Supplemental Figure 13. BLACAT2 overexpression promotes VEGF-C, SNAI2 and MMP9 expression in bladder cancer cells. (**A, B**) Quantitative RT-PCR quantification of VEGF-C, SNAI2 and MMP9 mRNA levels after BLACAT2 overexpression (A) or depletion (B). (**C, D**) ELISA quantification of secreted VEGF-C level after BLACAT2 overexpression (C) or depletion (D). Error bars

represent the standard deviation of the mean of three independent experiments. Statistical significance was assessed using two-tailed Student's t-tests (B and D) and one-way analyses of variance (ANOVA) followed by Dunnett's tests for multiple comparisons (A and C). ** $p<0.01$. (**E**) Immunoblot quantification of VEGF-C, SNAI2 and MMP9 protein levels after BLACAT2 overexpression or depletion in the 5637 cell line. Experiments were performed in three biological replicates.

Supplemental Figure 14. Correlation analyses of BLACAT2 and VEGF-C, SNAI2 and MMP9 expression. (**A**) BLACAT2 expression correlates with baseline VEGF-C expression in human bladder cancer cell lines. n=8. (**B**) Representative images of IHC staining showing that BLACAT2 expression positively correlates with VEGF-C, SNAI2 and MMP9 expression levels in the xenograft tumors. n=12 per group. Scale bars: 50 μm. (**C, D**) BLACAT2 expression positively correlates with VEGF-C, SNAI2 and MMP9 expression levels in xenograft tumors (C) and human bladder cancer tissues (D). n=12 per group for (C) and n=140 for (D). ** p<0.01.

Supplemental Figure 15. BLACAT2/VEGF-C promoter triplex sequences and CD spectrum of positive and negative control. (**A**) Triplex sequences formed by BLACAT2 and VEGF-C promoter predicted by Longtarget. (**B**) The CD spectrum of a 1:1 mixture of TFO in FENDRR with TTS in the PITX2 promoter sequence is shown in red, which was used as a positive control. The sum of individual TFO and TTS is shown in blue. (**C**) The CD spectrum of a 1:1 mixture of control single-stranded RNA (ssRNA) sequence with the PITX2 promoter sequence.

Supplemental Figure 16. BLACAT2 recruits WDR5 protein to the VEGF-C promoter and activates VEGF-C transcription. (**A, B**) ChIP-qPCR analysis of WDR5 genomic occupancy and H3K4 methylation status in the VEGF-C promoter

after overexpression (A) or depletion (B) of BLACAT2 in 5637 cells. An intronic sequence in the β-actin gene was used as a negative control. (**C, D**) ChIP-qPCR analysis of RNA pol II occupancy in the VEGF-C promoter after overexpression (C) or depletion (D) of BLACAT2 in UM-UC-3 and 5637 cells. Error bars represent the standard deviation of the mean of three independent experiments. Statistical significance was assessed using one-way analyses of variance (ANOVA) followed by Dunnett's tests for multiple comparisons. ** $p<0.01$.

Supplemental Figure 17. BLACAT2-regulated SNAI2 and MMP9 expression is not dependent on VEGF-C. (**A, B**) Quantitative RT-PCR quantification of SNAI2 and MMP9 mRNA levels after depletion of VEGF-C in BLACAT2-overexpressing bladder cancer cells. (**C**) Immunoblot quantification of VEGF-C, SNAI2 and MMP9 protein levels after depletion of VEGF-C in BLACAT2-overexpressing bladder cancer cells.

Supplemental Figure 18. MS identification of the BLACAT2-interacting protein as WDR5. (**A**) The most discriminative peaks (m/z signals) in MS. (**B-I**) The most discriminative peaks (m/z signals) in MS/MS.

Supplemental Figure 19. BLACAT2 regulates VEGF-C expression in bladder cancer cells with lower expression levels of WDR5. (**A**) Immunoblot quantification of baseline WDR5 expression levels in bladder cancer cell lines. (**B**) Quantitative RT-PCR and ELISA quantification of VEGF-C level after overexpression of wild-type or mutant BLACAT2 as indicated in bladder cancer cells. (**C, D**) ChIP-qPCR analysis of WDR5 genomic occupancy (C) and H3K4 methylation status (D) in the VEGF-C promoter after overexpression of BLACAT2. (**E**) ChIRP analysis of BLACAT2-associated chromatin in TCCSUP cells. Retrieved chromatin was

quantified by qPCR. The percent recovery of the input for ChIRP was calculated based on a 10% non-precipitated DNA sample for each experiment. The red arrows indicate the location of TTS. Error bars represent the standard deviation of the mean of three independent experiments. Statistical significance was assessed using one-way analyses of variance (ANOVA) followed by Dunnett's tests for multiple comparisons. ** $p<0.01$.

Supplemental Figure 20. WDR5 is required for BLACAT2-induced VEGF-C expression and lymphangiogenesis. (**A-C**) qRT-PCR (A), Western blot (B) and ELISA (C) analysis of WDR5 knockdown on BLACAT2-induced VEGF-C expression. (**D**) Representative images (left panel) and histogram quantification (right panel) of the tube formation assay with HLECs treated with conditioned medium derived from bladder cancer cells treated as indicated. WDR5 was depleted using siRNAs. Scale bars: 100 μm. (**E**) Representative images (left panel) and histogram quantification (right panel) of the transwell migration assay with HLECs cultured with conditioned medium derived from bladder cancer cells and treated as indicated. Scale bars: 200 μm. Error bars represent the standard deviation of three independent experiments. Statistical significance was assessed using two-tailed Student's t-tests (A and C) and one-way analyses of variance (ANOVA) followed by Dunnett's tests for multiple comparisons (D and E). ** $p<0.01$.

Supplemental Figure 21. BLACAT2 promotes VEGF-C expression and lymphangiogenesis in a SV-HUC-1 immortalized normal urothelial cell line model. (**A**) Overexpression (left panel) and knockdown (right panel) efficiencies of BLACAT2 or mutant BLACAT2 in SV-HUC-1 cells transduced with lentiviral vectors as indicated. (**B, C**) Histogram quantification of the tube formation assay and migration with HLECs. HLECs were cultured with conditioned medium derived from

SV-HUC-1 that were treated as indicated. (**D, E**) Histogram quantification of VEGF-C mRNA (D) and protein levels (E) in SV-HUC-1 cells transduced with lentiviral vectors as indicated. (**F**) ChIP-qPCR analysis of the WDR5 genomic occupancy and H3K4 methylation status in the VEGF-C promoter after overexpression of BLACAT2 in SV-HUC-1 cells. Error bars represent the standard deviation of the mean of three independent experiments. Statistical significance was assessed using one-way analyses of variance (ANOVA) followed by Dunnett's tests for multiple comparisons. ** $p<0.01$.

Supplemental Figure 22. BLACAT2 recruits WDR5 protein to the SNAI2 and MMP9 promoters. (**A, B**) ChIP-qPCR analysis of the WDR5 genomic occupancy (A) and H3K4 methylation status (B) in the SNAI2 and MMP9 promoters after overexpression of BLACAT2 in bladder cancer cells. An intronic sequence in the β-actin gene was used as a negative control. (**C**) ChIRP-qPCR analysis of BLACAT2-associated chromatin in UM-UC-3 cells. Retrieved chromatin was quantified by PCR. The percent recovery of the input for ChIRP was calculated based on a 10% non-precipitated DNA sample for each experiment. The red arrows indicate the location of TTS predicted by Longtarget. Error bars represent the standard deviation of the mean of three independent experiments. Statistical significance was assessed using one-way analyses of variance (ANOVA) followed by Dunnett's tests for multiple comparisons. ** $p<0.01$.

Supplemental Figure 23. Inhibition of VEGF-C abrogates BLACAT2-induced LN metastasis in vivo. (**A**) Representative images of popliteal LN metastasis after shRNA-mediated depletion of VEGF-C. Popliteal LNs were enucleated and analyzed until the mice died or after 60 days (n=12 per group). Scale bar: 5 mm. (**B**) Kaplan-Meier survival analysis of mice inoculated with the indicated cells. * $p<0.05$,

** p<0.01, Student's t-test.

Supplemental Figure 24. VEGF-C is required for BLACAT2-induced lymphangiogenesis in vitro. (**A**) Representative images (left panel) and quantification (right panel) of the Matrigel tube formation assay with HLECs. HLECs were treated with conditioned medium derived from bladder cancer cells treated as indicated, and VEGF-C was depleted using shRNAs. (**B**) Representative images (left panel) and histogram quantification (right panel) of transwell migration assays with HLECs cultured with conditioned medium derived from bladder cancer cells treated as indicated. VEGF-C was depleted with shRNAs. (**C, D**) Representative images (left panels) and histogram quantification (right panels) showing that overexpression of VEGF-C rescued the effect of BLACAT2 depletion on tube formation and HLEC migration. Scale bars: 200 μm. Error bars represent the standard deviation of the mean of three independent experiments. Statistical significance was assessed using two-tailed Student's t-tests (C and D) and one-way analyses of variance (ANOVA) followed by Dunnett's tests for multiple comparisons (A and B). ** p<0.01.

Supplemental Figure 25. Depletion of SNAI2 slightly inhibits BLACAT2-induced LN metastasis. (**A**) Knockdown efficiencies of SNAI2 in BLACAT2-transduced bladder cancer cells with lentiviral vectors as indicated. Error bars indicate the standard deviation of the mean, ** p<0.01, Student's t-test. (**B**) Representative images of enucleated popliteal LNs (left panel) and a histogram analysis of the LN volume is included (right panel). Scale bar: 5 mm. Error bars indicate the standard deviation of the mean, n=12. * p<0.05, Student's t-test. (**C**) The ratios of the metastatic to total enucleated popliteal LNs for the indicated group. (**D**) Representative images of the popliteal LNs analyzed by IHC staining using an anti-luciferase antibody (n=12 per group). Scale bars: black, 500 μm; red, 50 μm.

Supplemental Figure 26. VEGF-C is required for BLACAT2-induced lymphangiogenesis in vitro. (**A**) Representative images (left panel) and quantification (right panel) of the Matrigel tube formation assay with HLECs. HLECs were treated with conditioned medium derived from bladder cancer cells as indicated, and VEGF-C was depleted with a neutralizing antibody. Scale bars: 100 μm. (**B**) Representative images (left panel) and quantification (right panel) of the transwell migration assay with HLECs. Scale bars: 50 μm. Error bars represent the mean±SD of three independent experiments, ** $p<0.01$, Student's t-test.

Supplemental Figure 27. Inhibition of VEGF-C abrogates BLACAT2-induced LN metastasis in vivo. (**A**) Representative images of popliteal LNs after VEGF-C ablation using a neutralizing antibody (n=12 per group). Scale bar: 5 mm. (**B**) Kaplan-Meier survival analysis of mice inoculated with the indicated cells.

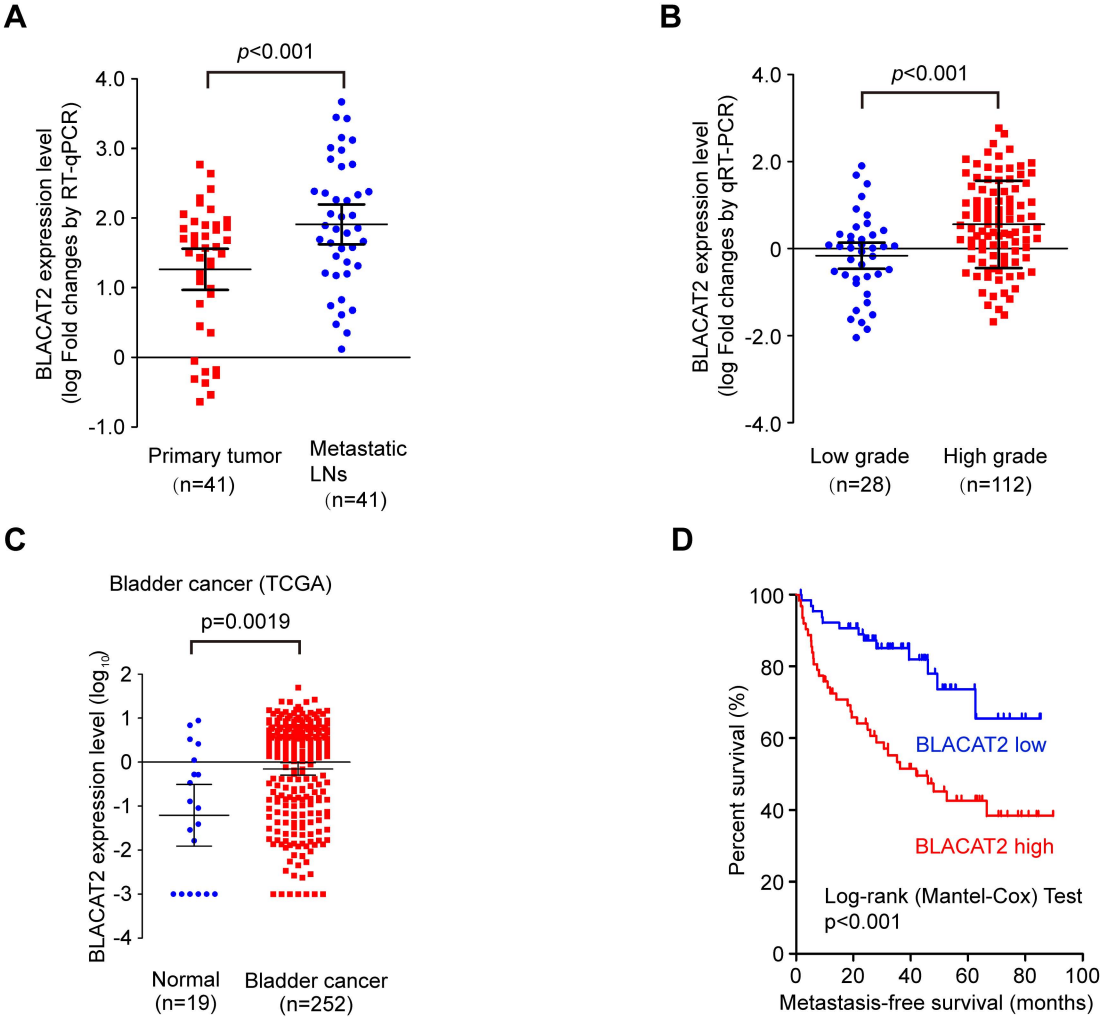

Supplemental Figure 1

BLACAT2 expression is overexpressed in high grade, metastatic bladder cancer and negatively correlates with prognosis. (A) Comparison of BLACAT2 expression in primary human bladder cancer samples and paired metastatic LNs. The nonparametric Mann-Whitney U test was used to compare the expression levels of the two groups. (B) QRT-PCR analysis of BLACAT2 expression in the 140-case cohort of freshly collected human bladder cancer samples with or without LN metastasis. (C) BLACAT2 expression in bladder cancer and normal urothelium from TCGA database. The nonparametric Mann-Whitney U test was used to compare the expression levels of the two groups. (D) Negative correlation between BLACAT2 expression and survival in the patient cohort referred to in Figure 1B. The Kaplan-Meier method was used to estimate survival for the 2 groups. The median BLACAT2 expression was used as a cutoff value.

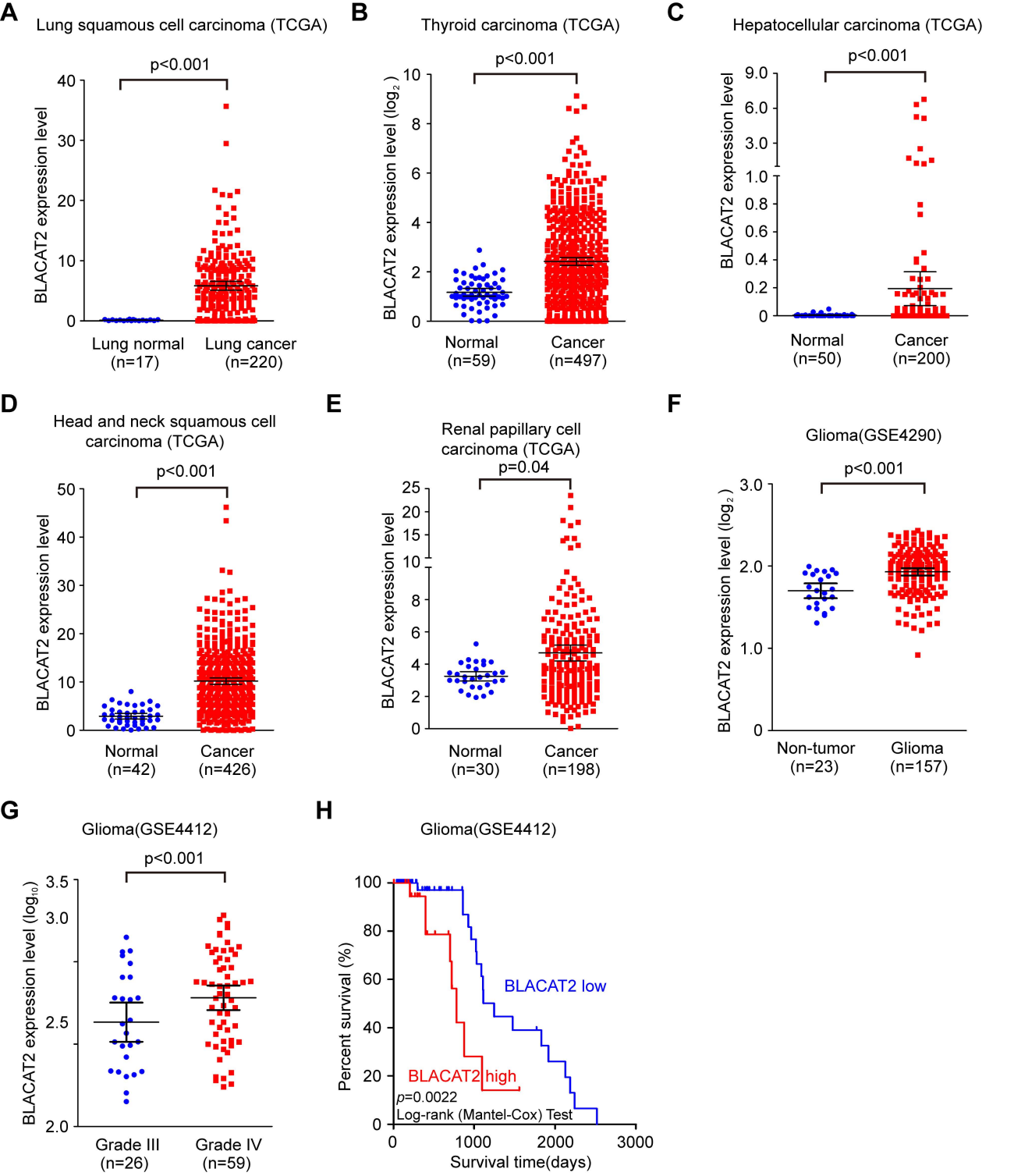

Supplemental Figure 2

BLACAT2 is overexpressed in multiple types of human cancer. (A-G) Data from the GEO and TCGA databases were analyzed in different types of cancers as indicated, including bladder cancer. The Mann-Whitney U test was used to compare differences between the two groups. Means with95% confidence intervalsare shown. (H) The GEO data showed that BLACAT2 overexpression correlates with a poor prognosis of glioma.

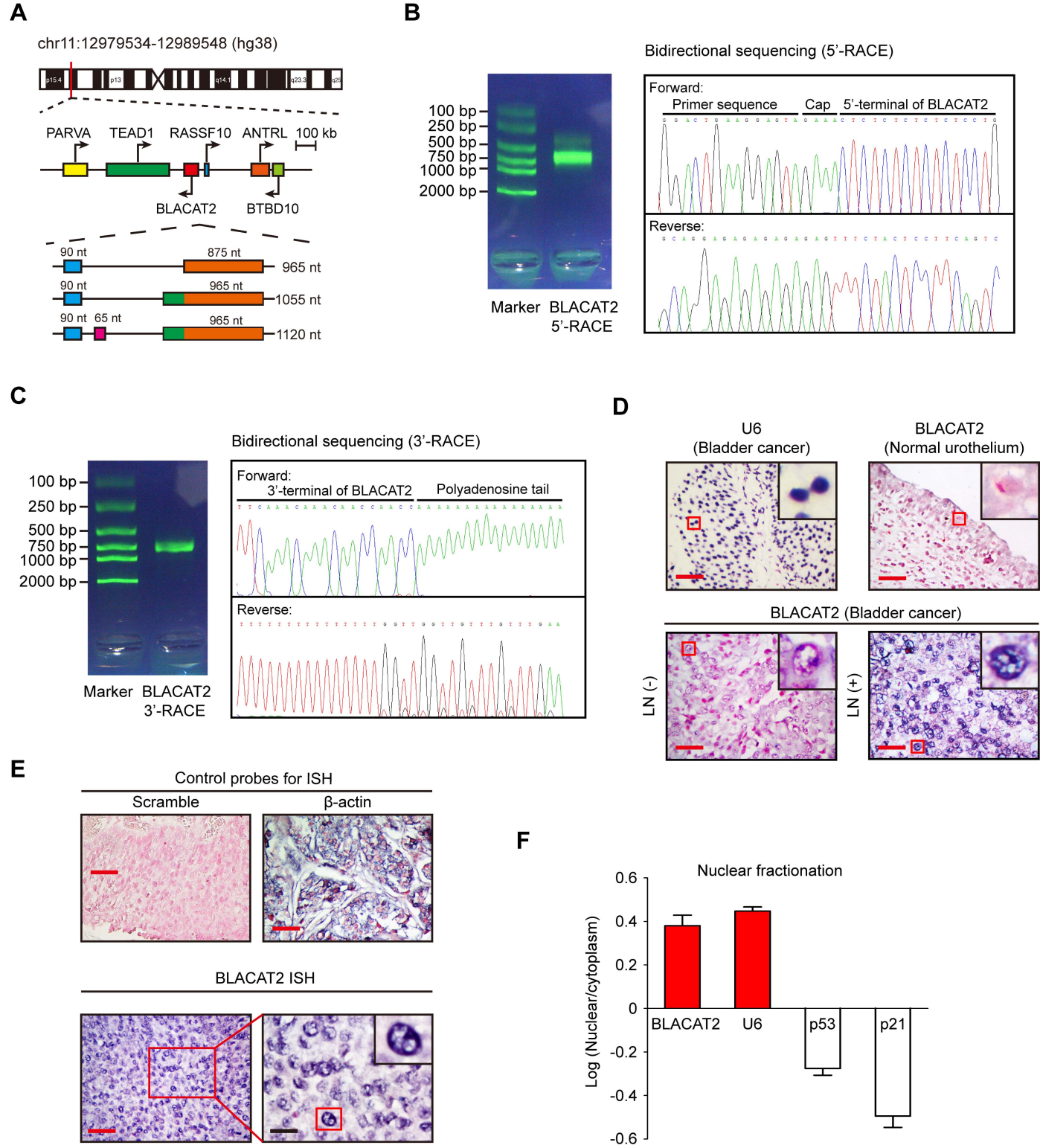

Supplemental Figure 3

BLACAT2 is localized in the nucleus in bladder cancer. (A) Schematic visualization of the chromosomal location of BLACAT2, its neighboring protein-coding genes and the alternative splicing isoforms of BLACAT2 determined using the RACE assay. (B) Representative image of agarose gel electrophoresis and bidirectional sequencing of the 5'-RACE products of BLACAT2 showing the cap sequence and 5'-terminal sequence of BLACAT2. At least 10 E.coli clones were sequenced. (C) Representative image of agarose gel electrophoresis and bidirectional sequencing of the 3'-RACE products of BLACAT2 showing the cap sequence and 3'-terminal sequence of BLACAT2. At least 10 E.coli clones were sequenced. (D) Representative images of the in situ hybridization (ISH) of BLACAT2 expression (blue) in the paraffin-embedded normal urothelium (n=20) and tumor sections of bladder cancer with or without LN metastasis (n=140). Samples were counterstained with nuclear fast red. The nuclear localized U6 probe was used as the technical positive control.(E, F) ISH analysis (E) and nuclear fractionation assay (F) showing that BLACAT2 preferentially localizes to the nucleus. Scramble probe served as the negative control, and β-actin served as the positive control in the cytoplasm.

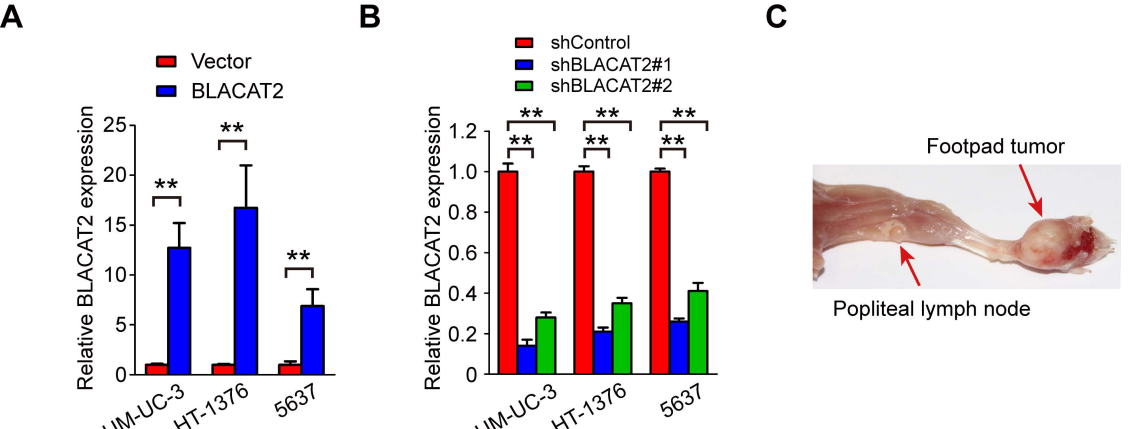

Supplemental Figure 4

Efficiencies of BLACAT2 overexpression and knockdown and representative image of popliteal LN metastasis model. (**A, B**) Quantitative RT-PCR analysis of BLACAT2 expression levels in BLACAT2-transduced, BLACAT2-silenced and control cells as indicated. The error bars indicate the standard deviation of the mean. Statistical significance was assessed using two-tailed Student's t-tests (A) and one-way analyses of variance (ANOVA) followed by Dunnett's tests for multiple comparisons (B). ** $p<0.01$. (**C**) Representative image of the nude mouse model of popliteal LN metastasis. UM-UC-3 cells transduced with according vectors were injected into the footpads of nude mice, and popliteal LNs were enucleated and analyzed until the mice died or after 60 days.

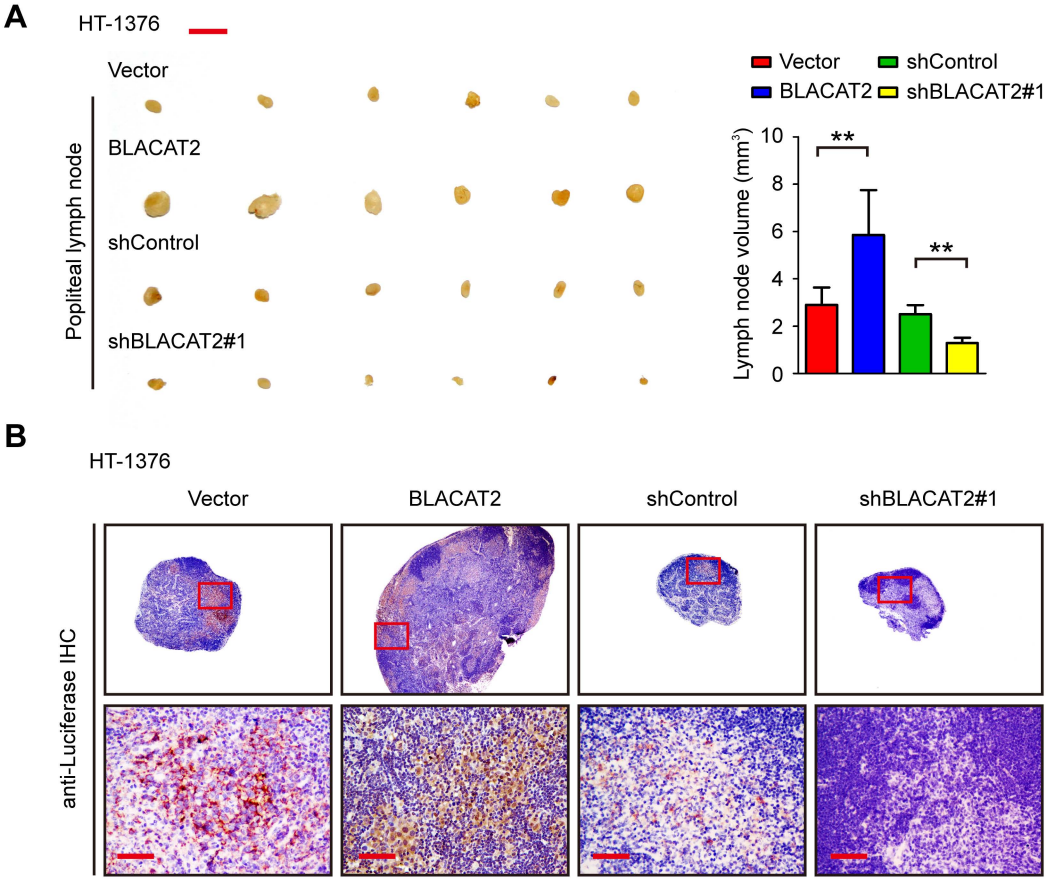

Supplemental Figure 5

BLACAT2 overexpression promotes LN metastasis of HT-1376 cells in vivo. (A) Representative images of enucleated popliteal LNs (left panel) after the overexpression or silencing of BLACAT2 as indicated are shown, and a histogram analysis of the LN volume is included (right panel). Scale bar: 5 mm. Error bars indicate the standard deviation of the mean, n=12. * $p<0.05$, ** $p<0.01$, Student's t-test. (B) Representative images of popliteal LNs analyzed by immunohistochemistry (IHC) staining with anti-luciferase antibody (n=12 per group). Scale bars: black, 500 μm; red, 50 μm.

A

BLACAT2 overexpression promoted popliteal lymph node metastasis in vivo

		No. total LNs	No. metastatic LNs	Metastatic ratio (%)
UM-UC-3 xenograft	Vector	12	4	33.3
	BLACAT2	12	12	100.0
	shControl	12	3	25.0
	shBLACAT2#1	12	0	0

BLACAT2 overexpression promoted popliteal lymph node metastasis in vivo

		No. total LNs	No. metastatic LNs	Metastatic ratio (%)
HT-1376 xenograft	Vector	12	4	33.3
	BLACAT2	12	12	100.0
	shControl	12	4	33.3
	shBLACAT2#1	12	0	0

B

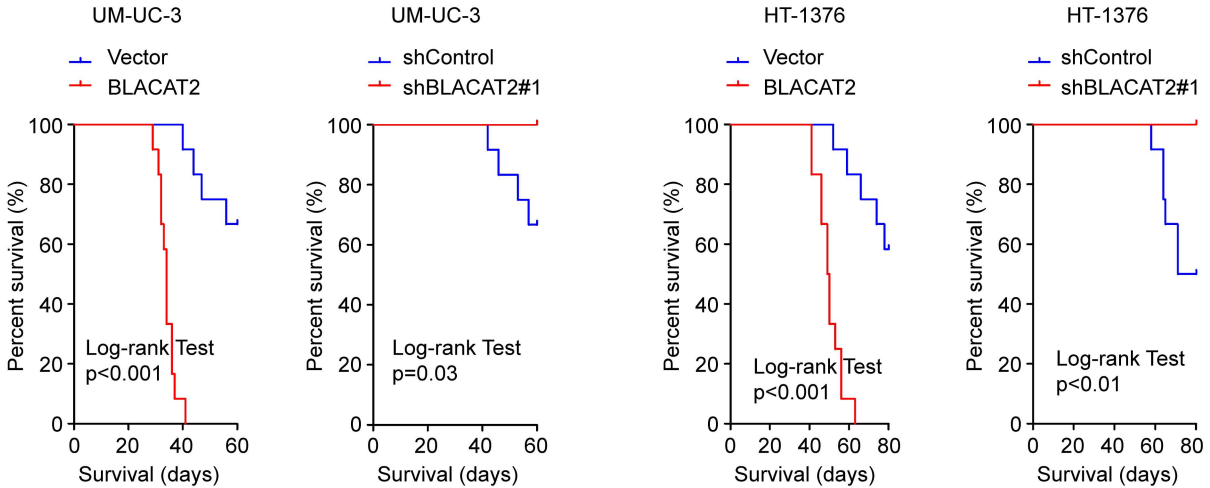

Supplemental Figure 6

BLACAT2 overexpression promotes LN metastasis and correlates with a poor prognosis in vivo. (A) The ratios of metastatic to total enucleated popliteal LNs for the indicated group. (B) Kaplan-Meier survival analysis of the mice (n=12 per group) that were inoculated with the indicated cells. The Kaplan-Meier (Mantel-Cox) test was used to evaluate the significant difference of the survival curves.

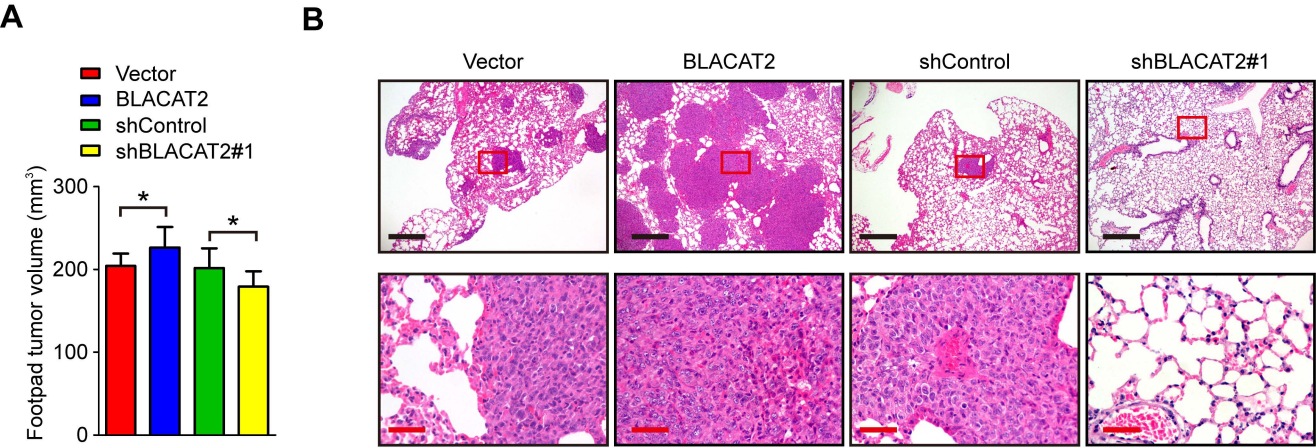

Supplemental Figure 7

BLACAT2 overexpression promotes lung metastasis. (**A**) Histogram analysis of the volumn of footpad tumor. UM-UC-3 cells were transduced with vectors as indicated. The error bars represent standard deviation of the mean, n=12, ** $p<0.01$, Student's t test. (**B**) Lung metastasis was confirmed by hematoxylin and eosin staining. Scale bars: black, 200 μm; red, 50 μm.

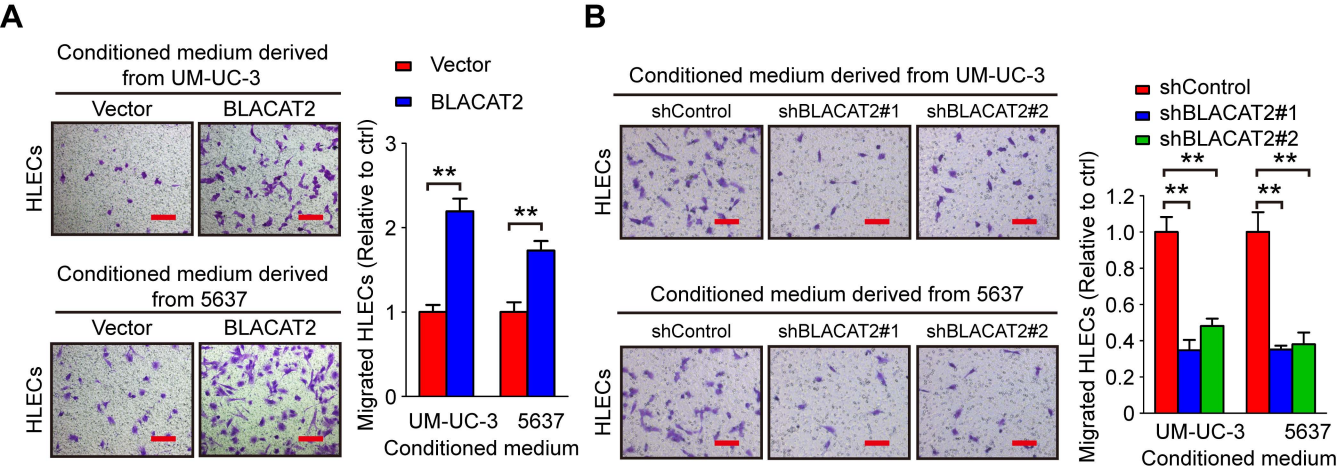

Supplemental Figure 8

BLACAT2 overexpression promotes HLECs migration. (**A, B**) Representative images (left panel) and histogram quantification (right panel) of Transwell migration assay with HLECs cultured with conditioned medium derived from bladder cancer cells after overexpression or knockdown of BLACAT2. Scale bars: 200 μm. All experiments in vitro were performed with at least three biological replicates. The error bars indicate the standard deviation of the mean. Statistical significance was assessed using two-tailed Student's t-tests (A) and one-way analyses of variance (ANOVA) followed by Dunnett's tests for multiple comparisons (B). ** $p<0.01$.

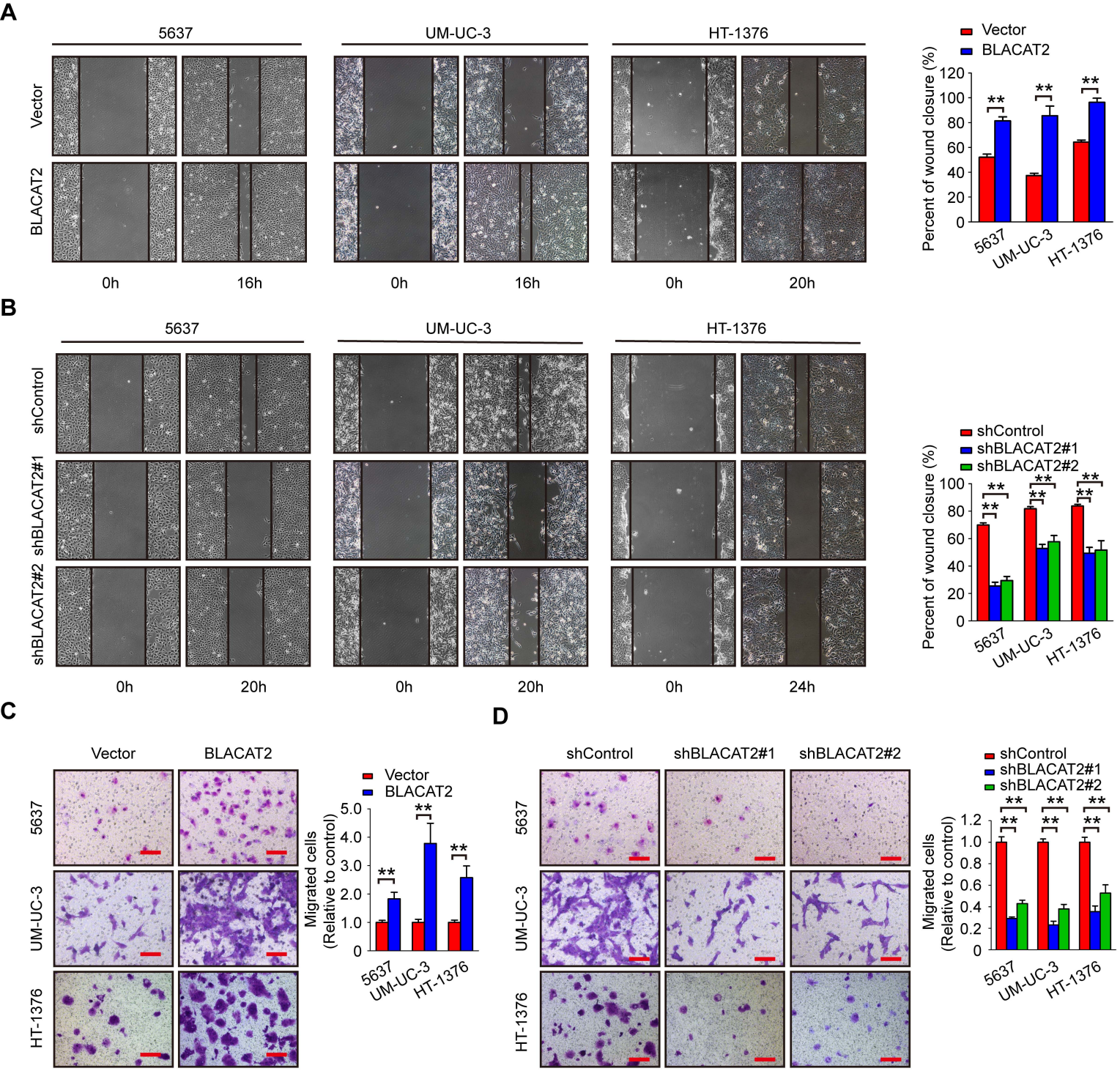

Supplemental Figure 9

BLACAT2 overexpression promotes bladder cancer cell migration. (A, B) Representative images of the woundhealing assay using bladder cancer cells (left panels) showing cell motility after ectopic expression (A) or knockdown (B) of BLACAT2 at the indicated time are shown, and a histogram analysis of the cell migration distance is provided (right panels). (C, D) Representative images of transwell migration assays of bladder cancer cells (left panels) showing cell motility after ectopic expression (C) or knockdown (D) of BLACAT2 are shown, and a histogram analysis of the migrated cell counts is provided (right panels). Error bars represent the standard deviation of the mean of three independent experiments. Scale bars: 200 μm. Statistical significance was assessed using two-tailed Student's t-tests (C) and one-way analyses of variance (ANOVA) followed by Dunnett's tests for multiple comparisons (A, B and D). ** p<0.01.

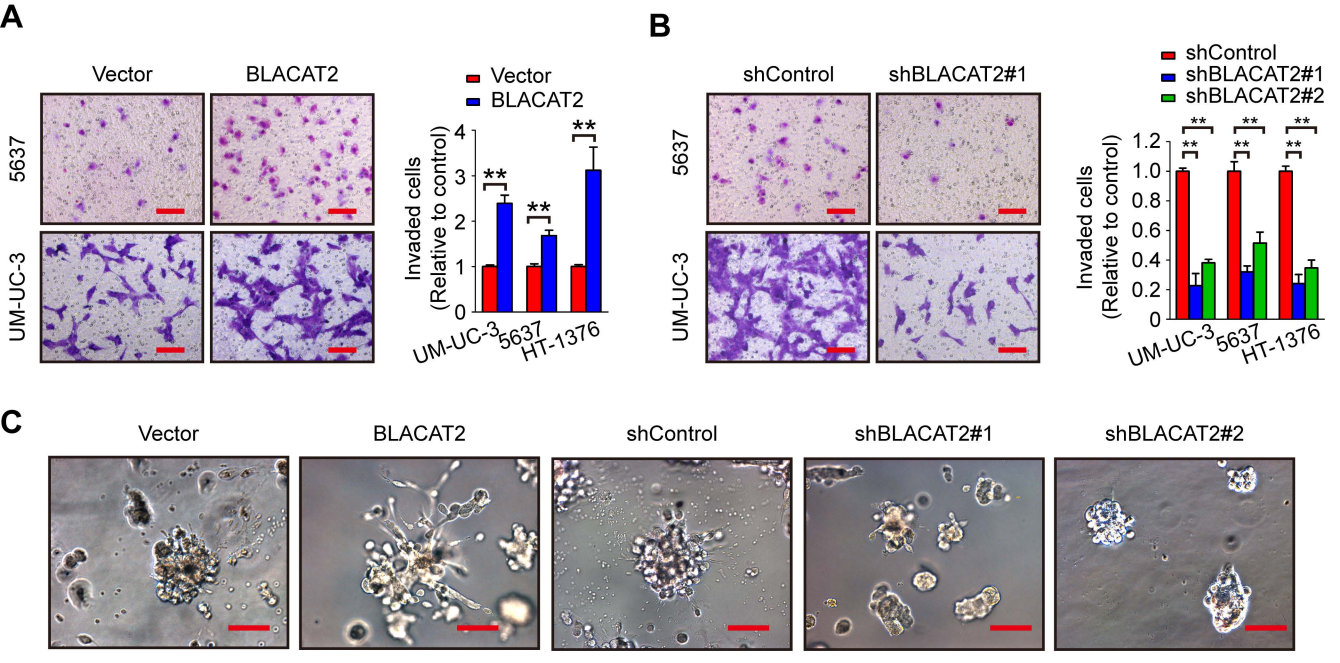

Supplemental Figure 10

BLACAT2 overexpression promotes invasiveness of bladder cancer cells. (**A, B**) Representative images (left panel) and histogram quantification (right panel) of the Matrigel invasion assay after BLACAT2 overexpression (A) and depletion (B), compared with the controls. Scale bars: 200 µm.(**C**) Representative images of the 3D culture of UM-UC-3 cells embedded in Matrigel for 5 days. Cells were treated as indicated. Scale bars: 50 µm. All experiments in vitro were performed with at least three biological replicates. The error bars indicate the standard deviation of the mean. Statistical significance was assessed using two-tailed Student's t-tests (A) and one-way analyses of variance (ANOVA) followed by Dunnett's tests for multiple comparisons (B). ** p<0.01.

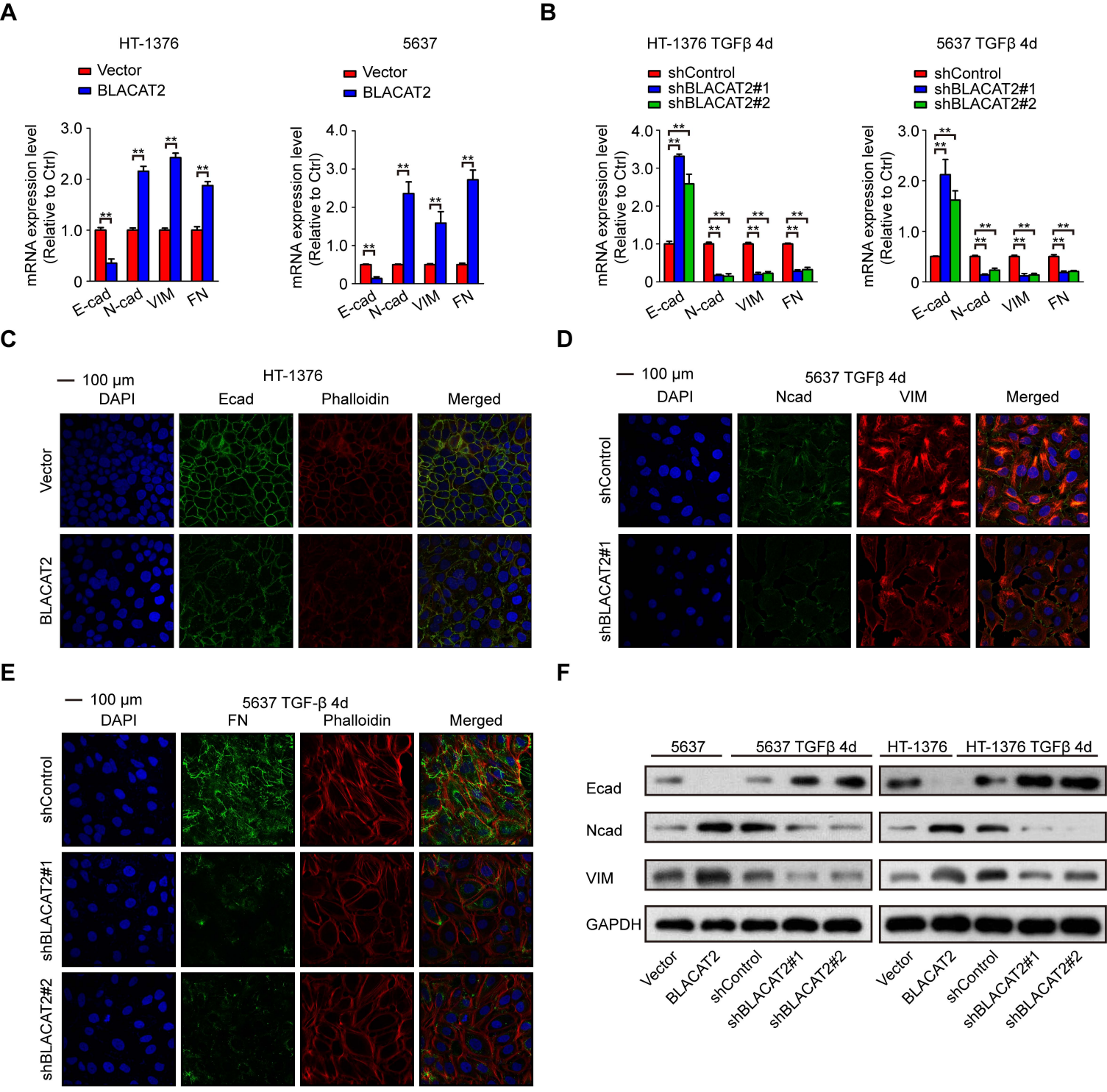

Supplemental Figure 11

BLACAT2 overexpression promotes EMT of bladder cancer cells. (A, B) Histogram analysis of the mRNA expression levels of EMT molecular biomarkers quantified by qRT-PCR after ectopic expression (A) or knockdown (B) of BLACAT2. Error bars represent the standard deviation of the mean of three independent experiments. Statistical significance was assessed using two-tailed Student's t-tests (A) and one-way analyses of variance (ANOVA) followed by Dunnett's tests for multiple comparisons (B). ** p<0.01. (C) Immunofluorescence showing E-cadherin expression and phalloidin staining showing cytoskeletal remodeling after BLACAT2 overexpression. (D, E) Immunofluorescence showing that depletion of BLACAT2 reverses TGF-β-induced up-regulation of the mesenchymal markers N-cadherin, vimentin (D) and fibronectin (E) and cytoskeletal remodeling as determined byphalloidin staining. (F) Western blot analysis of E-cadherin, N-cadherin and vimentin expression after overexpression or silencing of BLACAT2. TGF-β was used to induce EMT in5637 and HT-1376 epithelial cells.

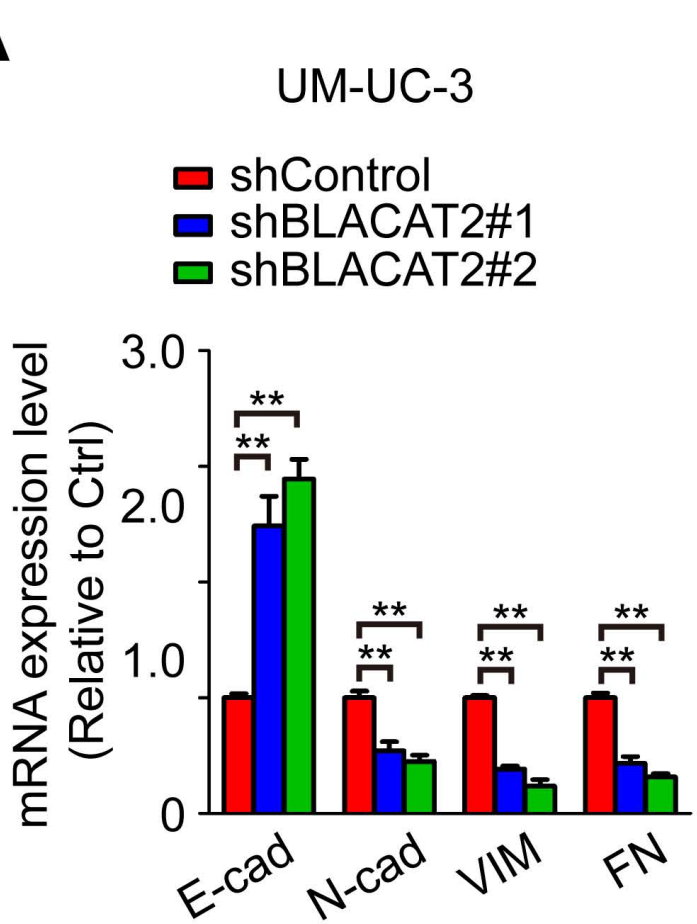

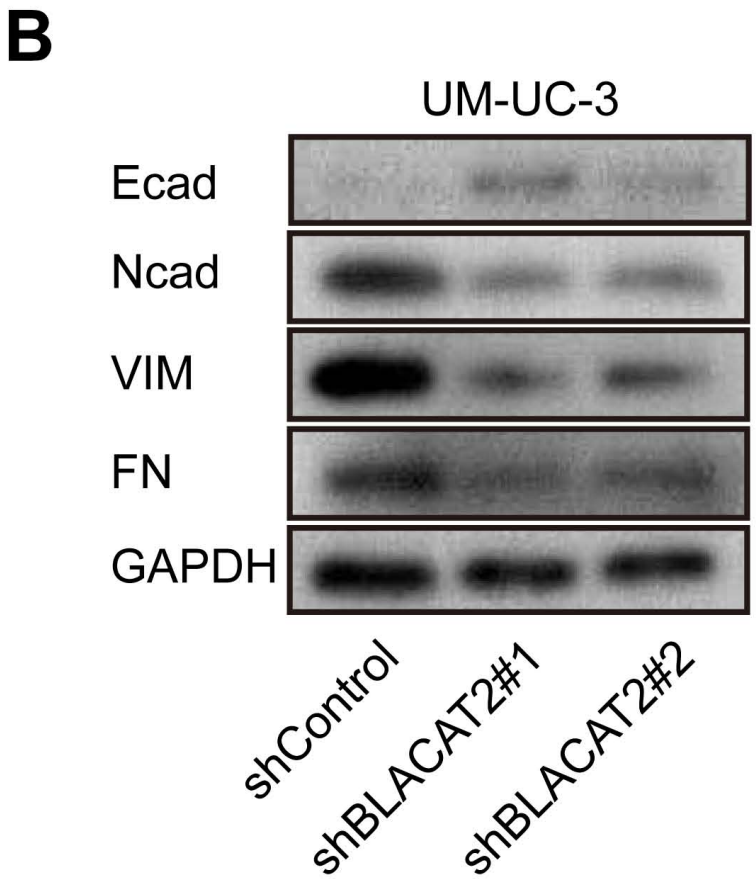

Supplemental Figure 12

BLACAT2 depletion partially reverses themesenchymal phenotype of UM-UC-3 bladder cancer cells at baseline. (**A**) Histogram analysis of the mRNA expression levels of EMT molecular biomarkers quantified by qRT-PCR after depletion of BLACAT2. Error bars represent the standard deviation of the mean of three independent experiments. Statistical significance was assessed using one-way analyses of variance (ANOVA) followed by Dunnett's tests for multiple comparisons. ** $p<0.01$. (**B**) Western blot analysis of E-cadherin, N-cadherin, fibronectin and vimentin expression after silencing of BLACAT2.

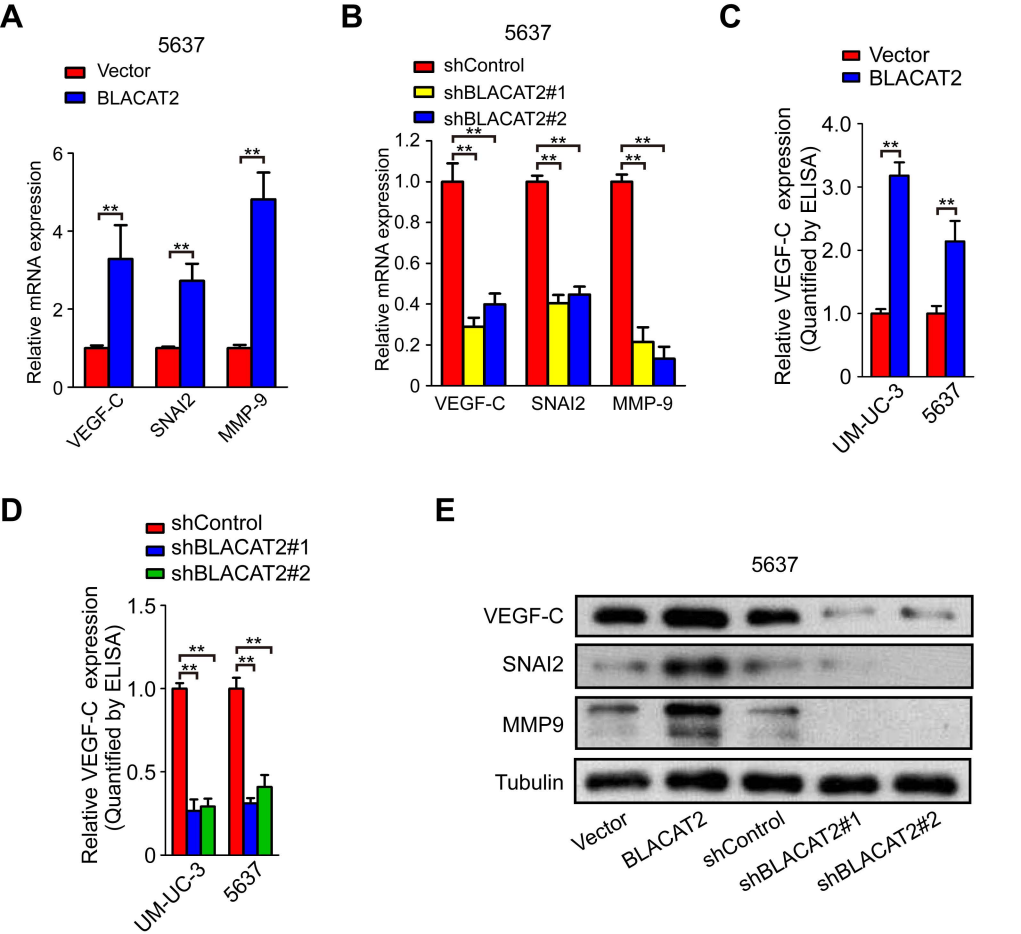

Supplemental Figure 13

BLACAT2 overexpression promotes VEGF-C, SNAI2 and MMP9 expression in bladder cancer cells. (A, B) Quantitative RT-PCR quantification of VEGF-C, SNAI2 and MMP9 mRNA levels after BLACAT2 overexpression (A) or depletion (B). (C, D) ELISA quantification of secreted VEGF-C level after BLACAT2 overexpression (C) or depletion (D). Error bars represent the standard deviation of the mean of three independent experiments. Statistical significance was assessed using two-tailed Student's t-tests (B and D) and one-way analyses of variance (ANOVA) followed by Dunnett's tests for multiple comparisons (A and C). ** p<0.01. (E) Immunoblot quantification of VEGF-C, SNAI2 and MMP9 protein levels after BLACAT2 overexpression or depletion in the 5637 cell line. Experiments were performed in three biological replicates.

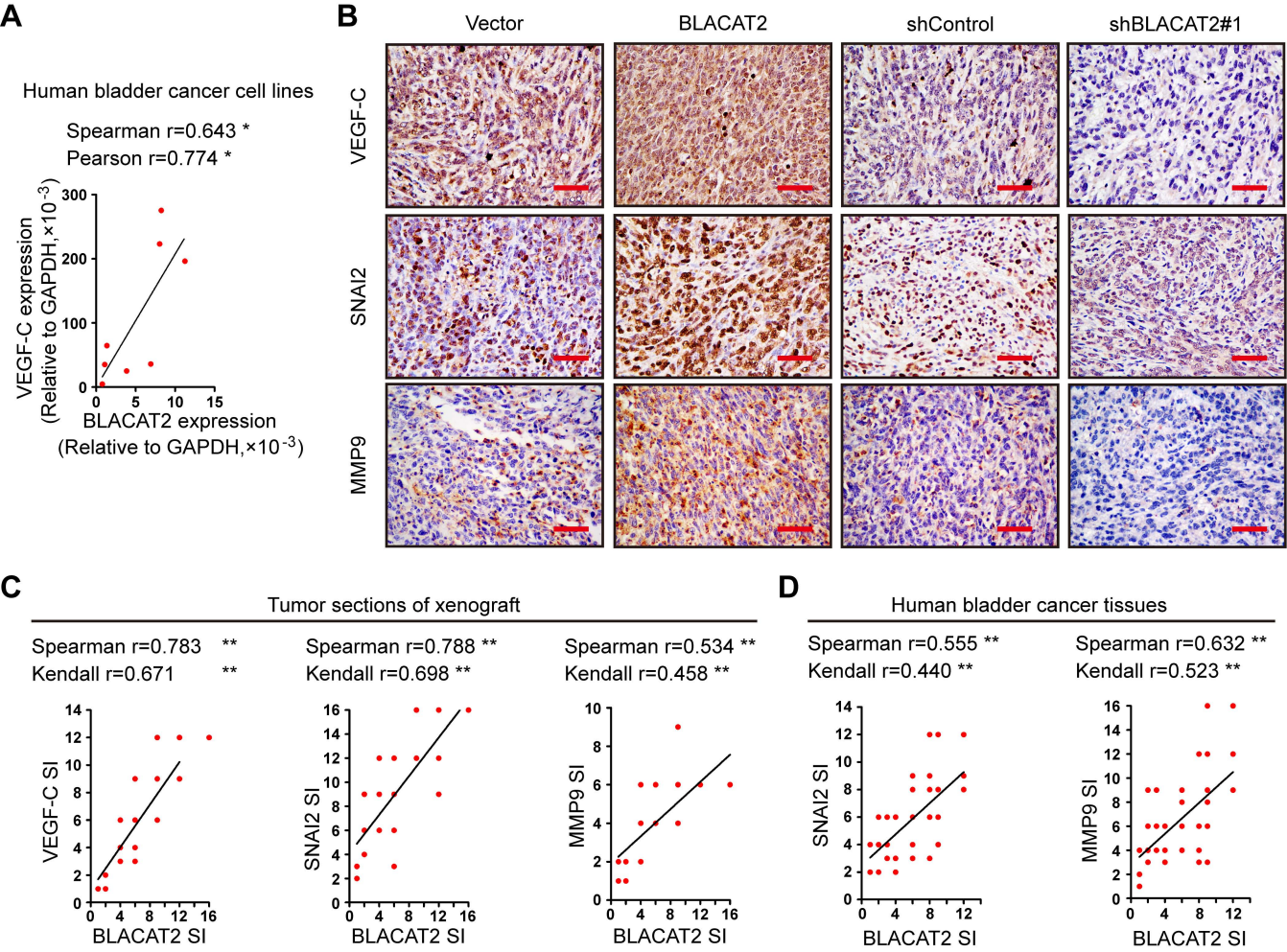

Supplemental Figure 14

Correlation analyses of BLACAT2 and VEGF-C, SNAI2 and MMP9 expression. (A) BLACAT2 expression correlates with baseline VEGF-C expression in human bladder cancer cell lines. n=8. (B) Representative images of IHC staining showing that BLACAT2 expression positively correlates with VEGF-C, SNAI2 and MMP9 expression levels in the xenograft tumors. n=12 per group. Scale bars: 50 μm. (C, D) BLACAT2 expression positively correlates with VEGF-C, SNAI2 and MMP9 expression levels in xenograft tumors (C) and human bladder cancer tissues (D). n=12 per group for (C) and n=140 for (D). ** p<0.01.

A

BLACAT2/VEGF-C promoter triplex sequences predicted by Longtarget:

	Triplex forming oligo (TFO) sequences		Triplex target site (TTS) sequences	Mean Stability	Strand
TFO1	5'-TGCTTCCCTCTCACCCTCTGCAG TTTCC-3'	TTS1	5'-AAGAACTCGGGAGTGGCCGAGG ATAAAGC-3'	2.92	ParaPus
TFO2	5'-CTGCTTGCTTCCCTCTCACCCTC TGCAGTTTCCT-3'	TTS2	5'-CATCAATAAAGGGAGTGAACAGCC ACACAGAATGGA-3'	2.59	ParaPlus

B

PITX2 5'-TTCTCCCTCCCCTCCATCCT CTTCCTTCTCCTCCTCCTCTT-3'

FENDRR 5'-GAGGAGGAGGAGGAGGAGGA GGAGGAGGAGGAGGAGGAGGA-3'

Positive control:

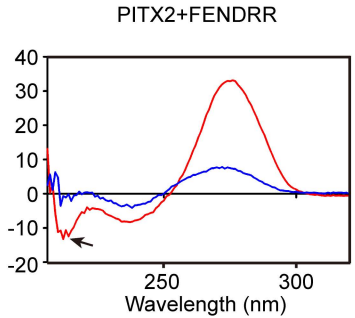

C

PITX2 5'-TTCTCCCTCCCCTCCATCCT CTTCCTTCTCCTCCTCCTCTT-3'

Control ssRNA 5'-AGTCTGCACAGTGAGCAATAC GAGCTCAAGCCAGTCTCGCA-3'

Negative control:

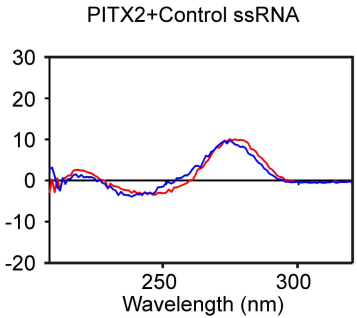

Supplemental Figure 15

BLACAT2/VEGF-C promoter triplex sequences and CD spectrum of positive and negative control. (A) Triplex sequences formed by BLACAT2 and VEGF-C promoter predicted by Longtarget. (B) The CD spectrum of a 1:1 mixture of TFO in FENDRR with TTS in the PITX2 promoter sequence is shown in red, which was used as a positive control. The sum of individual TFO and TTS is shown in blue. (C) The CD spectrum of a 1:1 mixture of control single-stranded RNA (ssRNA) sequence with the PITX2 promoter sequence.

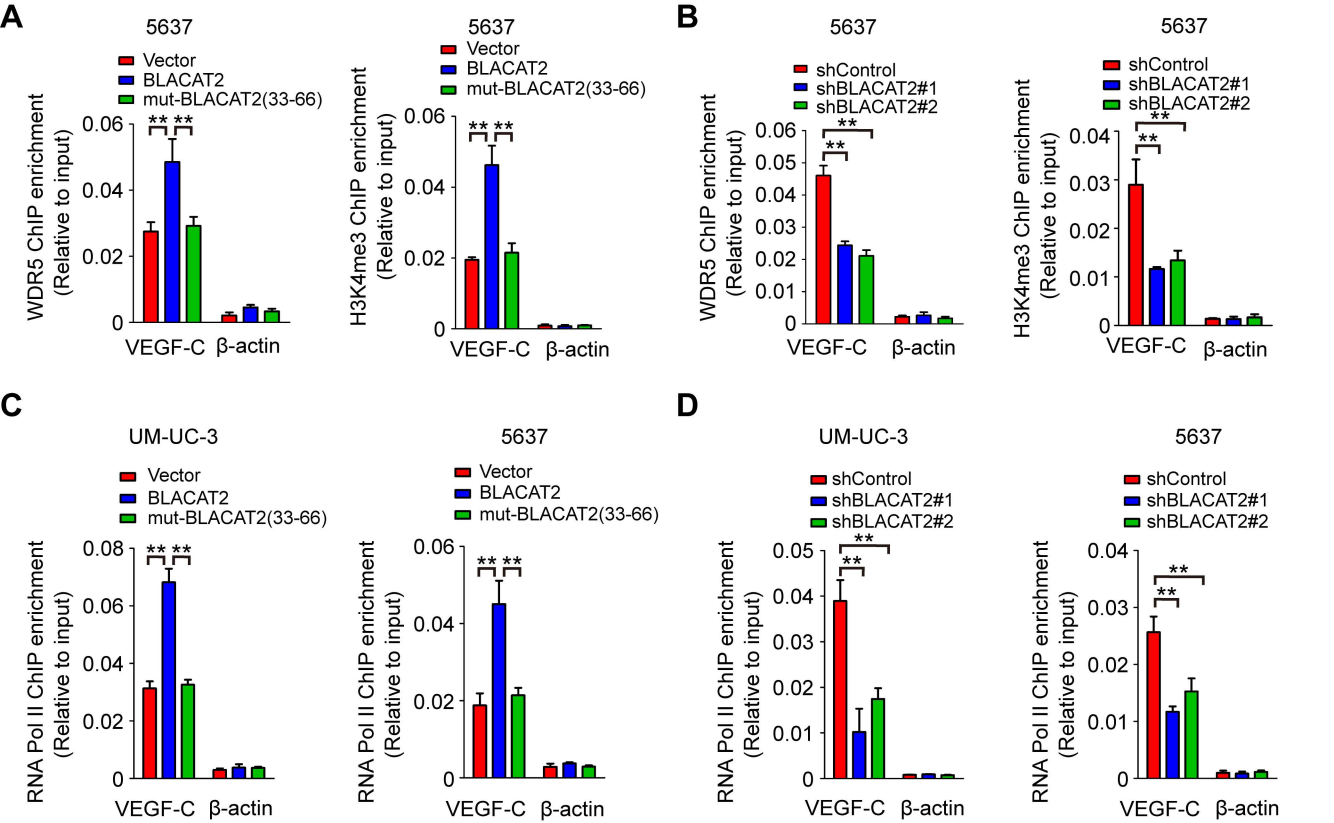

Supplemental Figure 16

BLACAT2 recruits WDR5 protein to the VEGF-C promoter and activates VEGF-C transcription. (A, B) ChIP-qPCR analysis of WDR5 genomic occupancy and H3K4 methylation status in the VEGF-C promoter after overexpression (A) or depletion (B) of BLACAT2 in 5637 cells. An intronic sequence in the β-actin gene was used as a negative control. (C, D) ChIP-qPCR analysis of RNA pol II occupancy in the VEGF-C promoter after overexpression (C) or depletion (D) of BLACAT2 in UM-UC-3 and 5637 cells. Error bars represent the standard deviation of the mean of three independent experiments. Statistical significance was assessed using one-way analyses of variance (ANOVA) followed by Dunnett's tests for multiple comparisons. ** $p<0.01$.

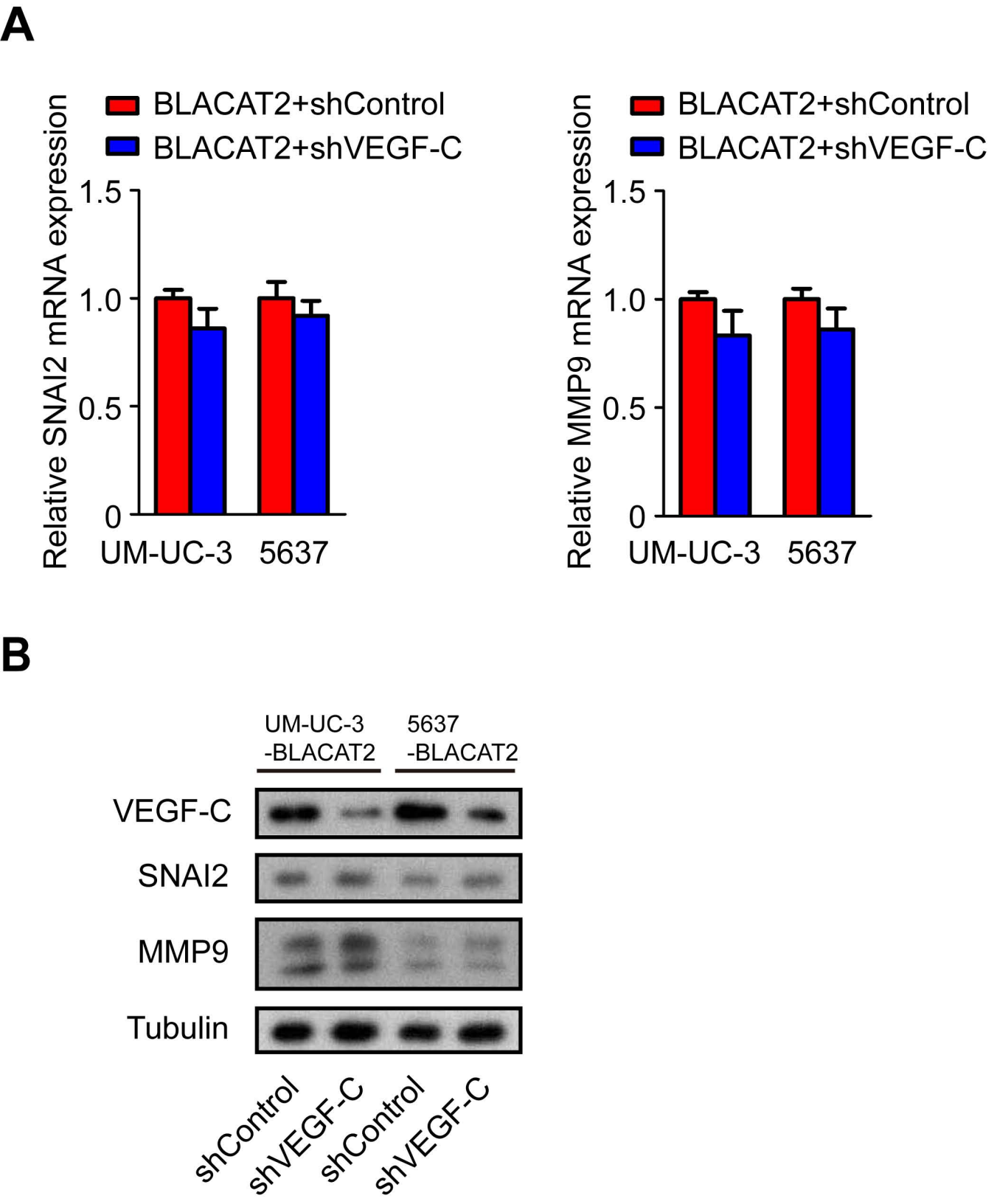

Supplemental Figure 17
BLACAT2-regulated SNAI2 and MMP9 expression is not dependent on VEGF-C. (A, B) Quantitative RT-PCR quantification of SNAI2 and MMP9 mRNA levels after depletion of VEGF-C in BLACAT2-overexpressing bladder cancer cells. (C) Immunoblot quantification of VEGF-C, SNAI2 and MMP9 protein levels after depletion of VEGF-C in BLACAT2-overexpressing bladder cancer cells.

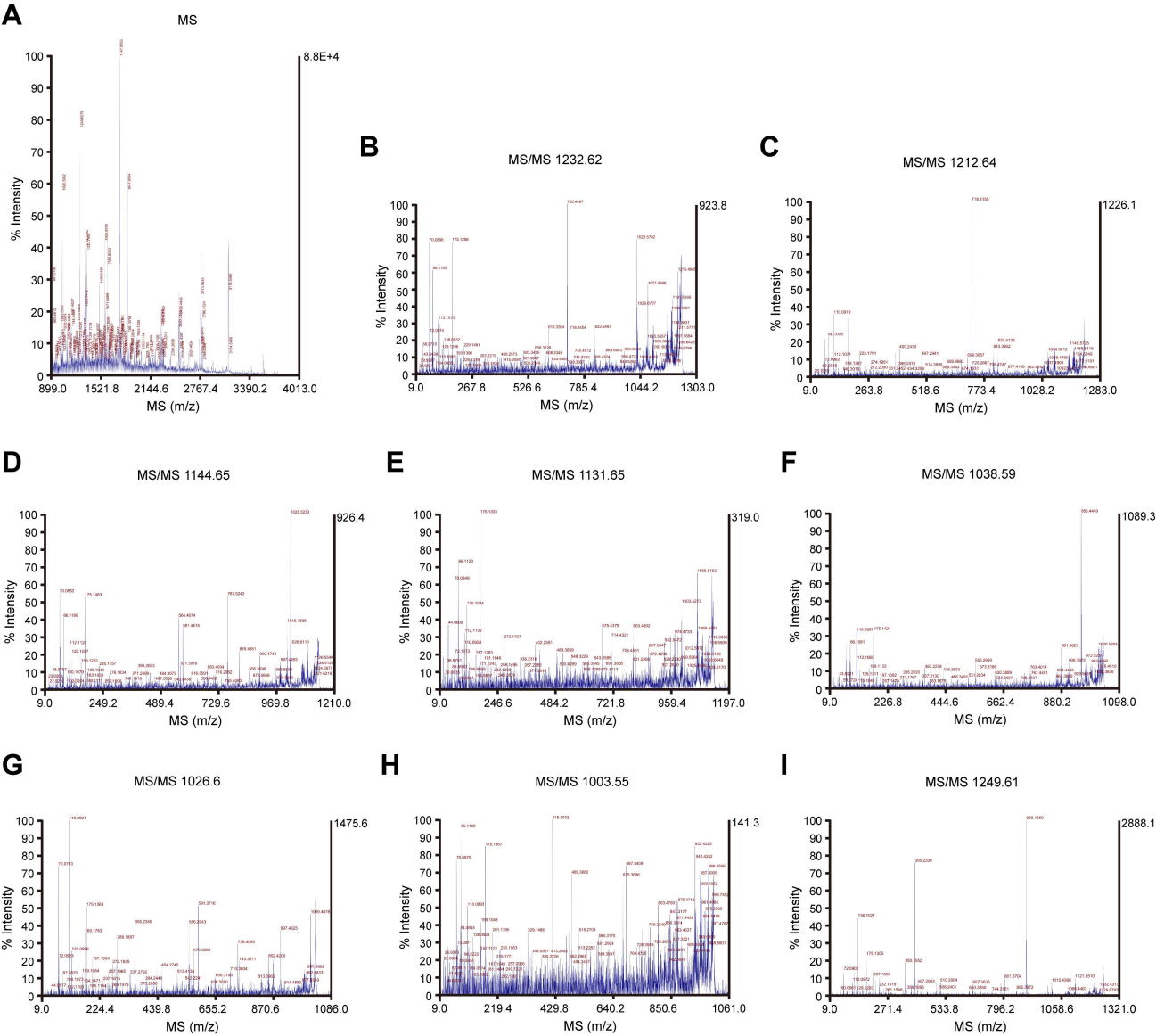

Supplemental Figure 18

MS identification of the BLACAT2-interacting protein as WDR5. (A) The most discriminative peaks (m/z signals) in MS. (B-I) The most discriminative peaks (m/z signals) in MS/MS.

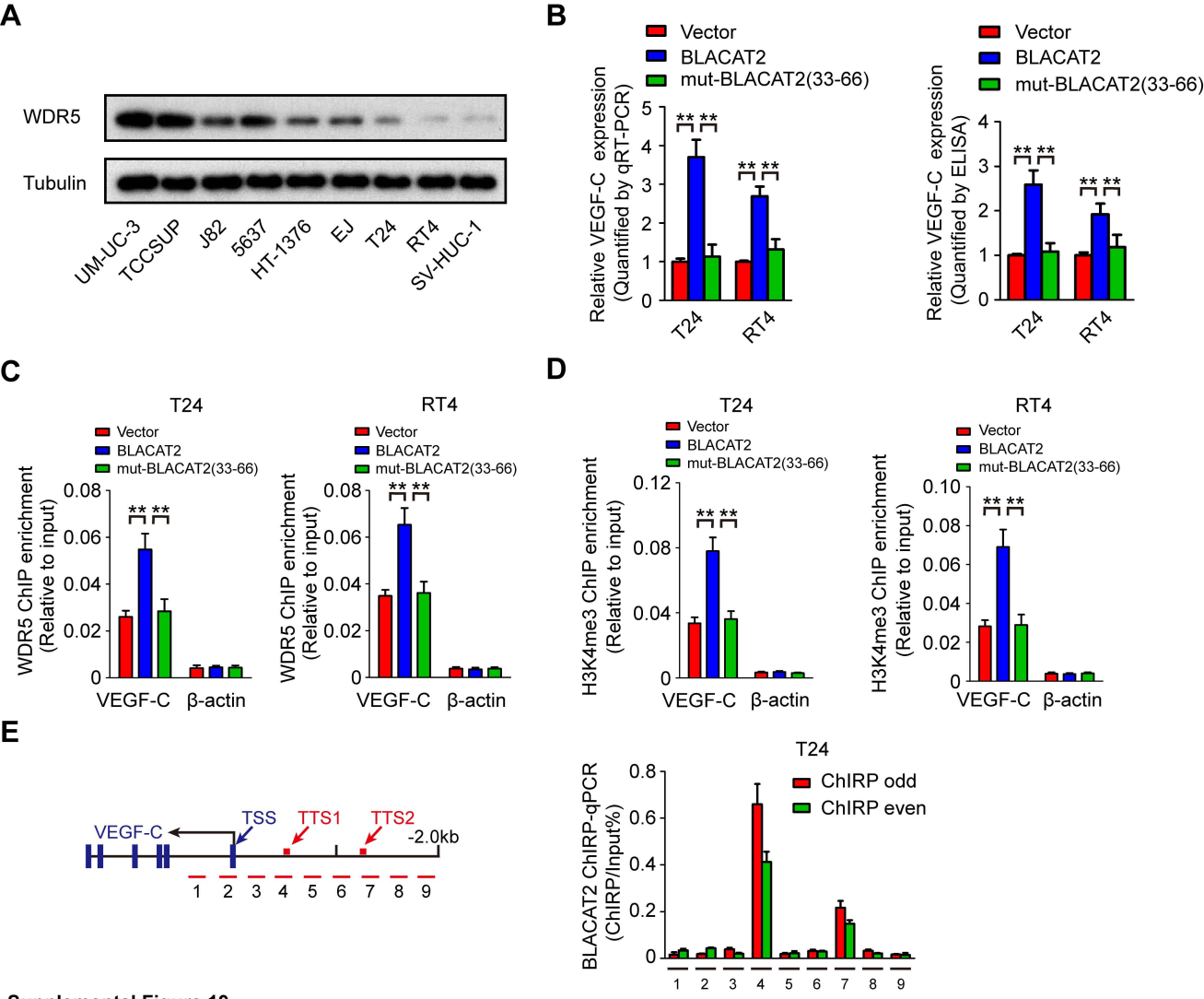

Supplemental Figure 19

BLACAT2 regulates VEGF-C expression in bladder cancer cells with lower expression levels of WDR5. (A) Immunoblot quantification of baseline WDR5 expression levels in bladder cancer cell lines. (B) Quantitative RT-PCR and ELISA quantification of VEGF-C level after overexpression of wild-type or mutant BLACAT2 as indicated in bladder cancer cells. (C, D) ChIP-qPCR analysis of WDR5 genomic occupancy (C) and H3K4 methylation status (D) in the VEGF-C promoter after overexpression of BLACAT2. (E) ChIRP analysis of BLACAT2-associated chromatin in TCCSUP cells. Retrieved chromatin was quantified by qPCR. The percent recovery of the input for ChIRP was calculated based on a 10% non-precipitated DNA sample for each experiment. The red arrows indicate the location of TTS. Error bars represent the standard deviation of the mean of three independent experiments. Statistical significance was assessed using one-way analyses of variance (ANOVA) followed by Dunnett's tests for multiple comparisons. ** p<0.01.

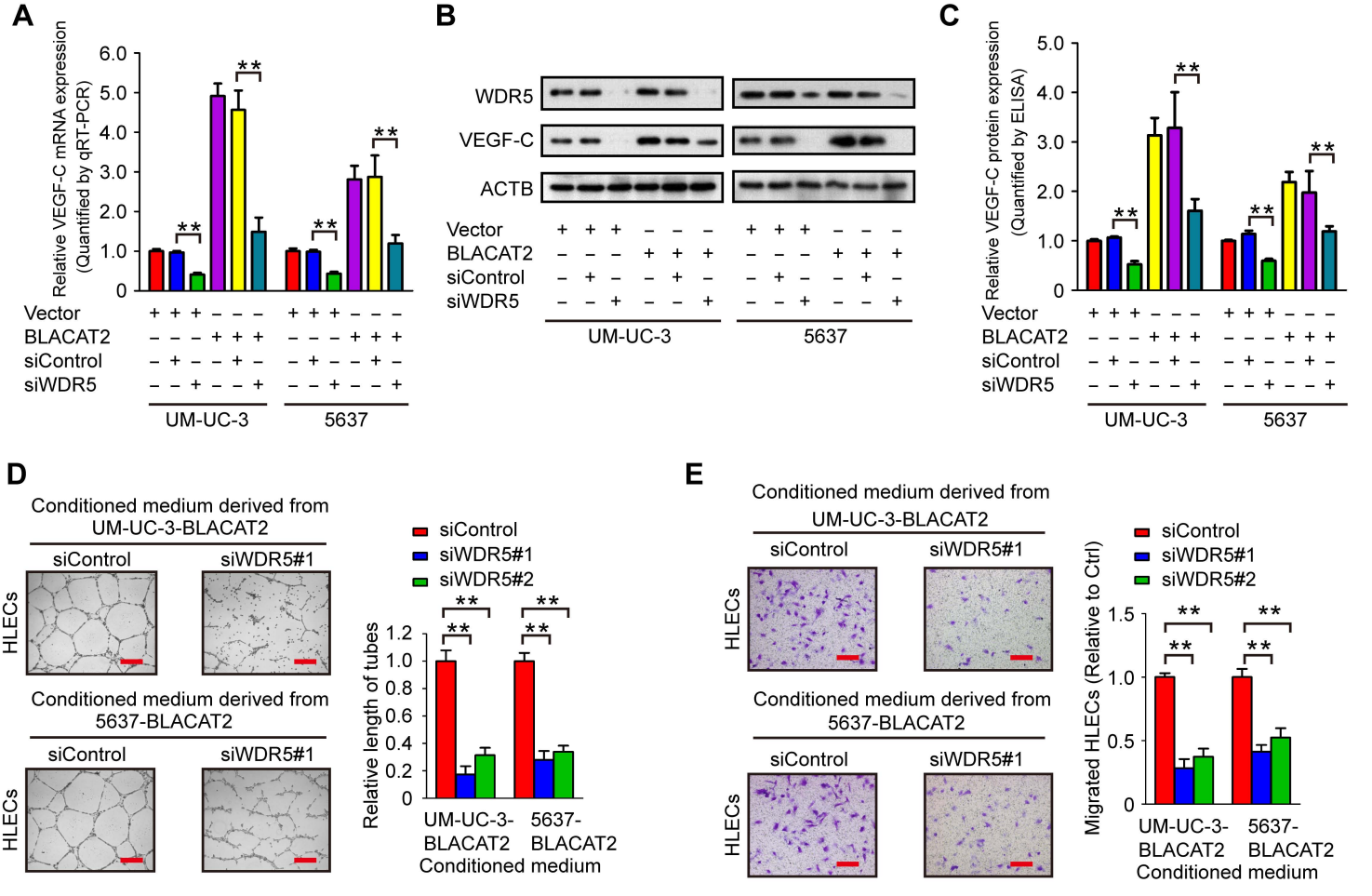

Supplemental Figure 20

WDR5 is required for BLACAT2-induced VEGF-C expression and lymphangiogenesis. (A-C) qRT-PCR (A), Western blot (B) and ELISA (C) analysis of WDR5 knockdown on BLACAT2-induced VEGF-C expression. (D) Representative images (left panel) and histogram quantification (right panel) of the tube formation assay with HLECs treated with conditioned medium derived from bladder cancer cells treated as indicated. WDR5 was depleted using siRNAs. (E) Representative images (left panel) and histogram quantification (right panel) of the transwell migration assay with HLECs cultured with conditioned medium derived from bladder cancer cells and treated as indicated. Scale bars: 200 μm. Error bars represent the standard deviation of three independent experiments. Statistical significance was assessed using two-tailed Student's t-tests (A and C) and one-way analyses of variance (ANOVA) followed by Dunnett's tests for multiple comparisons (D and E). ** $p<0.01$.

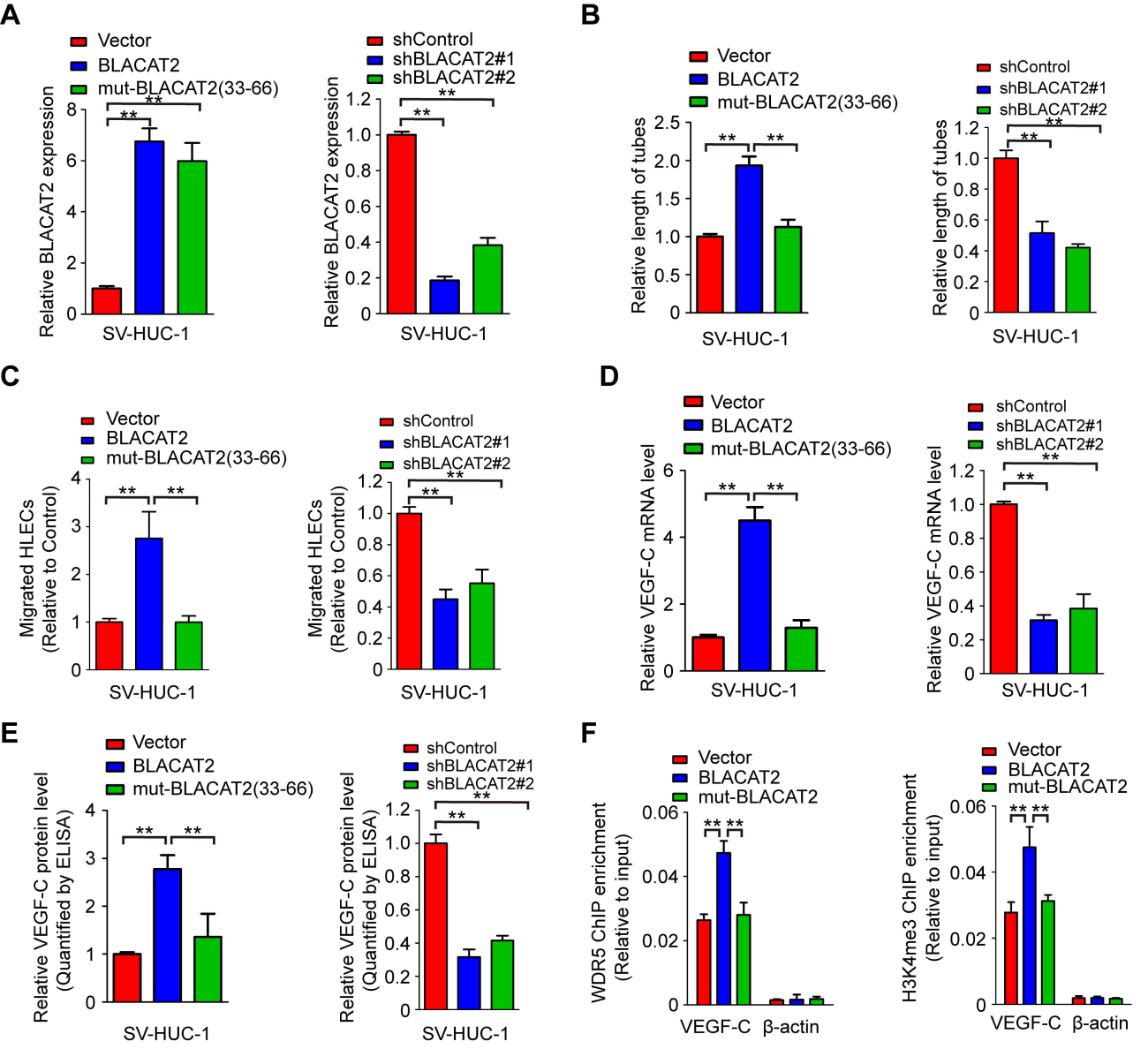

Supplemental Figure 21

BLACAT2 promotes VEGF-C expression and lymphangiogenesis in a SV-HUC-1 immortalized normal urothelial cell line model. (A) Overexpression (left panel) and knockdown (right panel) efficiencies of BLACAT2 or mutant BLACAT2 in SV-HUC-1 cells transduced with lentiviral vectors as indicated. (B, C) Histogram quantification of the tube formation assay and migration with HLECs. HLECs were cultured with conditioned medium derived from SV-HUC-1 that were treated as indicated. (D, E) Histogram quantification of VEGF-C mRNA (D) and protein levels (E) in SV-HUC-1 cells transduced with lentiviral vectors as indicated. (F) ChIP-qPCR analysis of the WDR5 genomic occupancy and H3K4 methylation status in the VEGF-C promoter after overexpression of BLACAT2 in SV-HUC-1 cells. Error bars represent the standard deviation of the mean of three independent experiments. Statistical significance was assessed using one-way analyses of variance (ANOVA) followed by Dunnett's tests for multiple comparisons. ** $p<0.01$.

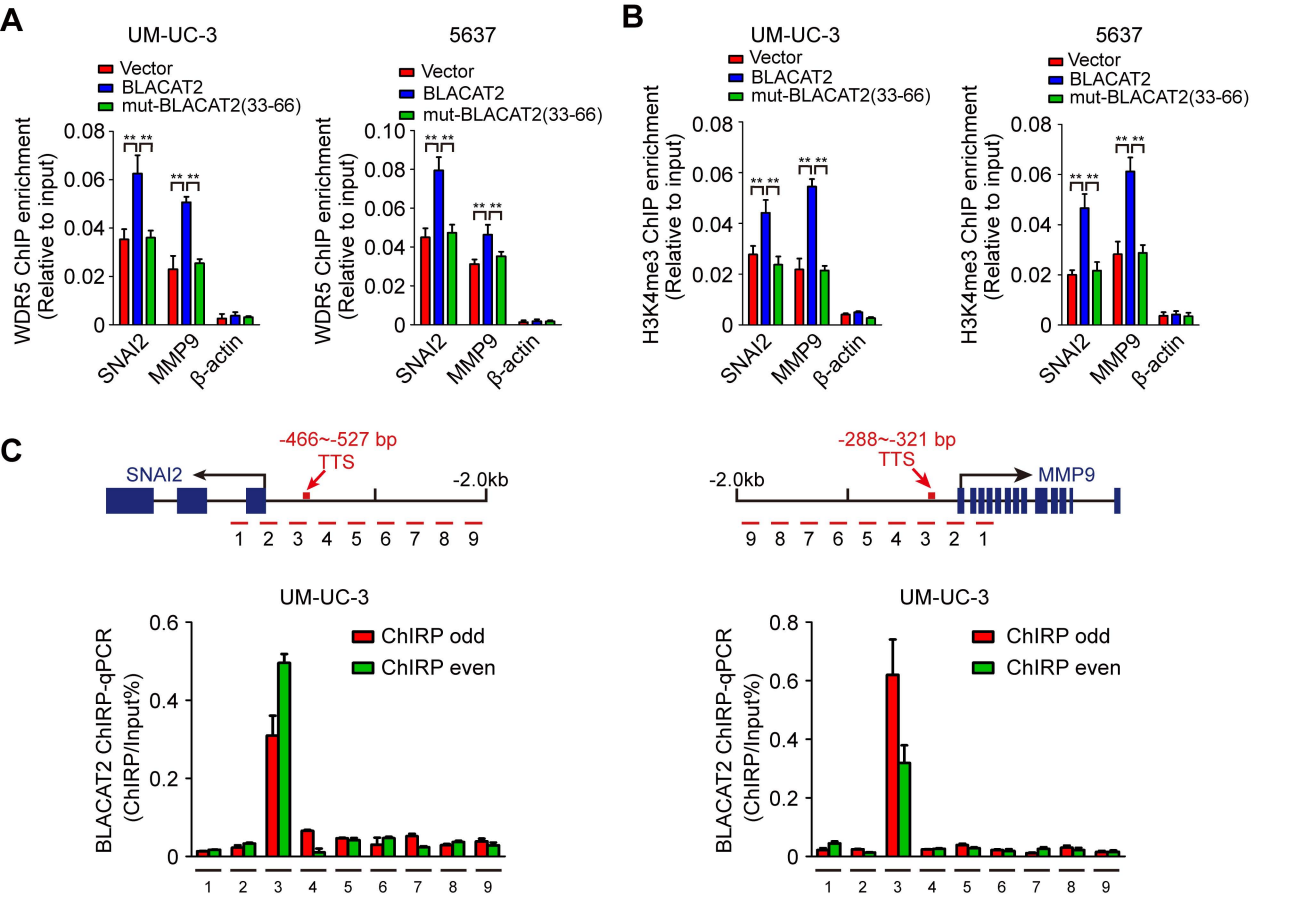

Supplemental Figure 22

BLACAT2 recruits WDR5 protein to the SNAI2 and MMP9 promoters. (A, B) ChIP-qPCR analysis of the WDR5 genomic occupancy (A) and H3K4 methylation status (B) in the SNAI2 and MMP9 promoters after overexpression of BLACAT2 in bladder cancer cells. An intronic sequence in the β-actin gene was used as a negative control. (C) ChIRP-qPCR analysis of BLACAT2-associated chromatin in UM-UC-3 cells. Retrieved chromatin was quantified by PCR. The percent recovery of the input for ChIRP was calculated based on a 10% non-precipitated DNA sample for each experiment. The red arrows indicate the location of TTS predicted by Longtarget. Error bars represent the standard deviation of the mean of three independent experiments. Statistical significance was assessed using one-way analyses of variance (ANOVA) followed by Dunnett's tests for multiple comparisons. ** $p<0.01$.

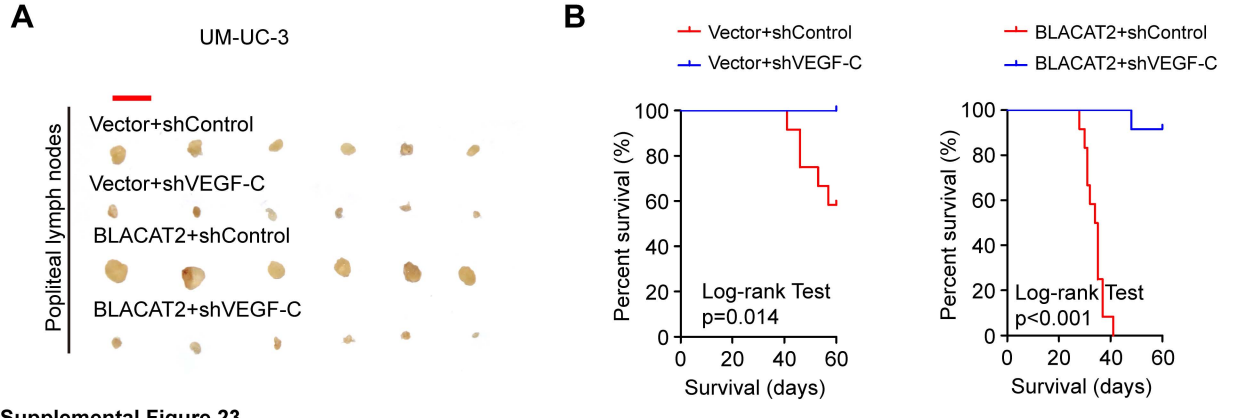

Supplemental Figure 23

Inhibition of VEGF-C abrogates BLACAT2-induced LN metastasis in vivo. (A) Representative images of popliteal LN metastasis after shRNA-mediated depletion of VEGF-C. Popliteal LNs were enucleated and analyzed until the mice died or after 60 days (n=12 per group). Scale bar: 5 mm. (B) Kaplan-Meier survival analysis of mice inoculated with the indicated cells. * p<0.05, ** p<0.01, Student's t-test.

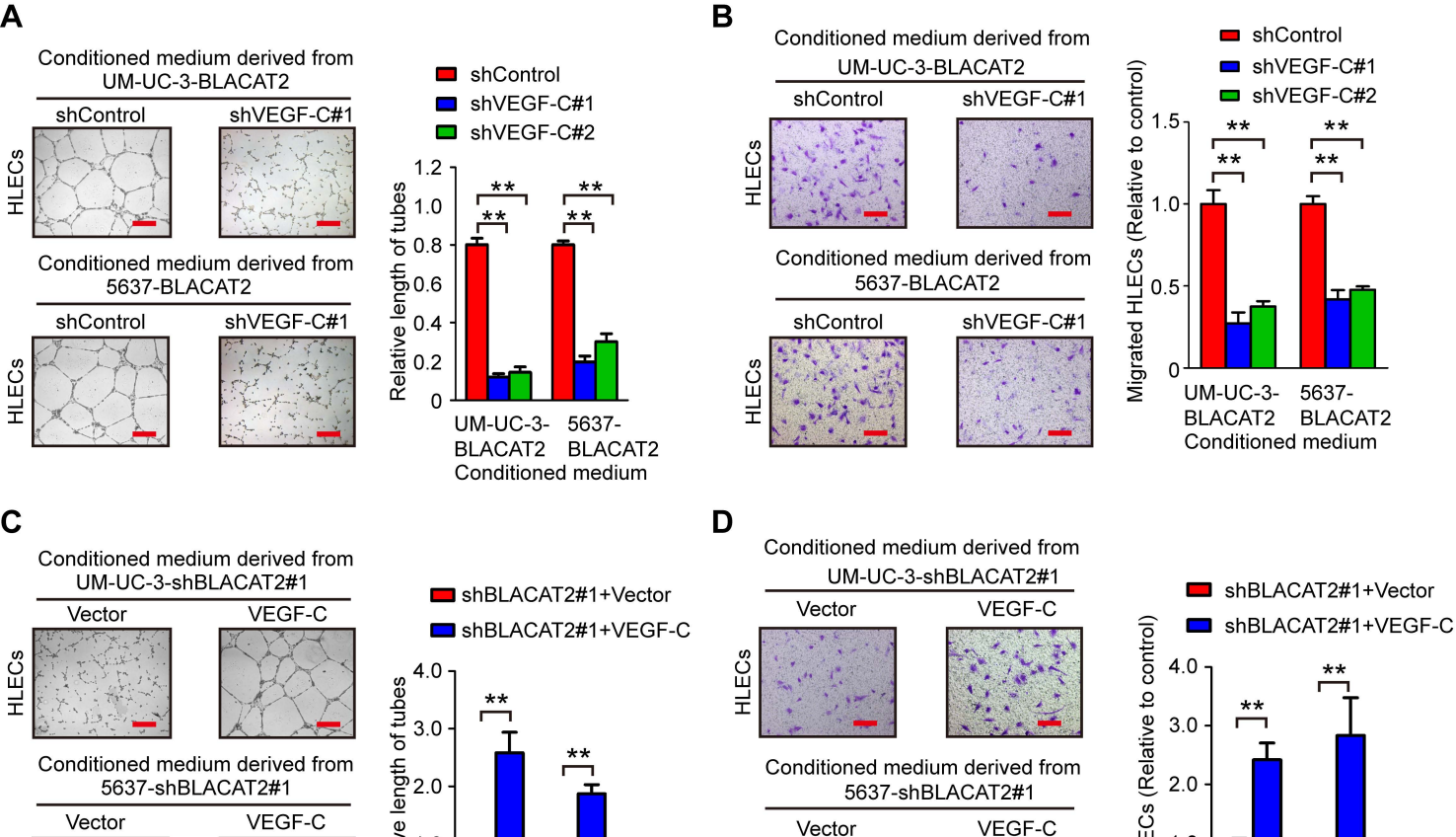

Supplemental Figure 24

VEGF-C is required for BLACAT2-induced lymphangiogenesis in vitro. (A) Representative images (left panel) and quantification (right panel) of the Matrigel tube formation assay with HLECs. HLECs were treated with conditioned medium derived from bladder cancer cells treated as indicated, and VEGF-C was depleted using shRNAs. (B) Representative images (left panel) and histogram quantification (right panel) of transwell migration assays with HLECs cultured with conditioned medium derived from bladder cancer cells treated as indicated. VEGF-C was depleted with shRNAs. (C, D) Representative images (left panels) and histogram quantification (right panels) showing that overexpression of VEGF-C rescued the effect of BLACAT2 depletion on tube formation and HLEC migration. Scale bars: 200 μm. Error bars represent the standard deviation of the mean of three independent experiments. Statistical significance was assessed using two-tailed Student's t-tests (C and D) and one-way analyses of variance (ANOVA) followed by Dunnett's tests for multiple comparisons (A and B). ** $p<0.01$.

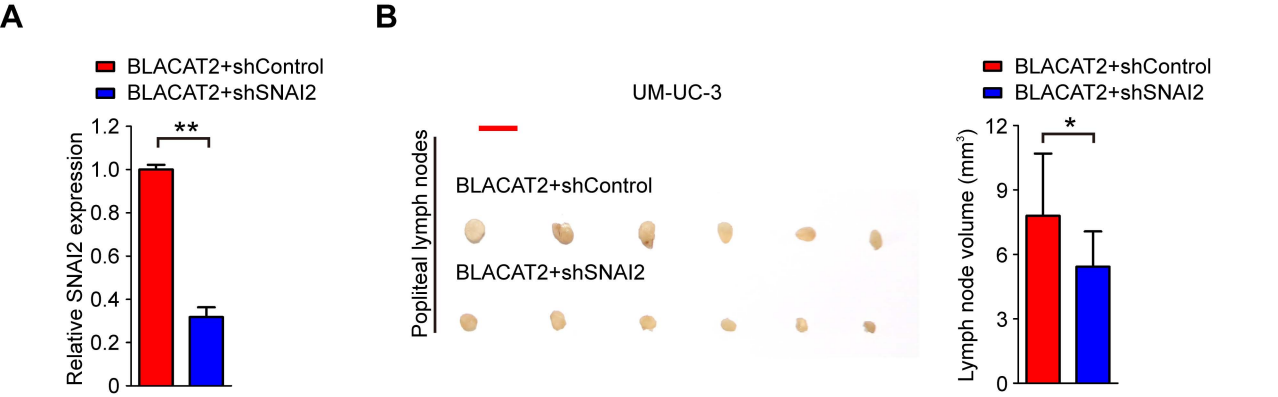

C

Popliteal lymph node metastasis in vivo

	No. total LNs	No. metastatic LNs	Metastatic ratio (%)
BLACAT2+shControl	12	12	100
BLACAT2+shSNAI2	12	10	83

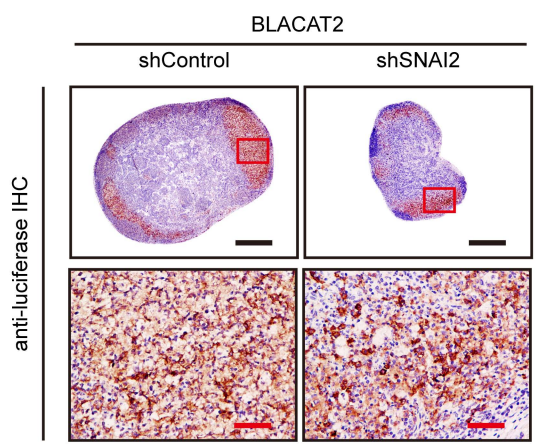

Supplemental Figure 25

Depletion of SNAI2 slightly inhibits BLACAT2-induced LN metastasis. (A) Knockdown efficiencies of SNAI2 in BLACAT2-transduced bladder cancer cells with lentiviral vectors as indicated. Error bars indicate the standard deviation of the mean, ** $p<0.01$, Student's t-test. (B) Representative images of enucleated popliteal LNs (left panel) and a histogram analysis of the LN volume is included (right panel). Scale bar: 5 mm. Error bars indicate the standard deviation of the mean, n=12. * $p<0.05$, Student's t-test. (C) The ratios of the metastatic to total enucleated popliteal LNs for the indicated group. (D) Representative images of the popliteal LNs analyzed by IHC staining using an anti-luciferase antibody (n=12 per group). Scale bars: black, 500 μm; red, 50 μm.

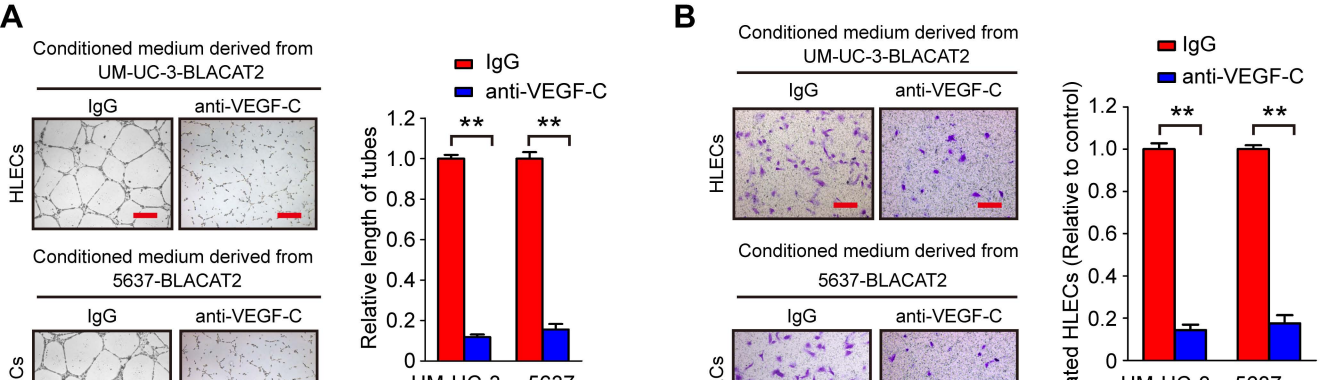

Supplemental Figure 26

VEGF-C is required for BLACAT2-induced lymphangiogenesis in vitro. (A) Representative images (left panel) and quantification (right panel) of the Matrigel tube formation assay with HLECs. HLECs were treated with conditioned medium derived from bladder cancer cells as indicated, and VEGF-C was depleted with a neutralizing antibody. Scale bars: 100 μm. (B) Representative images (left panel) and quantification (right panel) of the transwell migration assay with HLECs. Scale bars: 50 μm. Error bars represent the mean±SD of three independent experiments, ** $p<0.01$, Student's t-test.

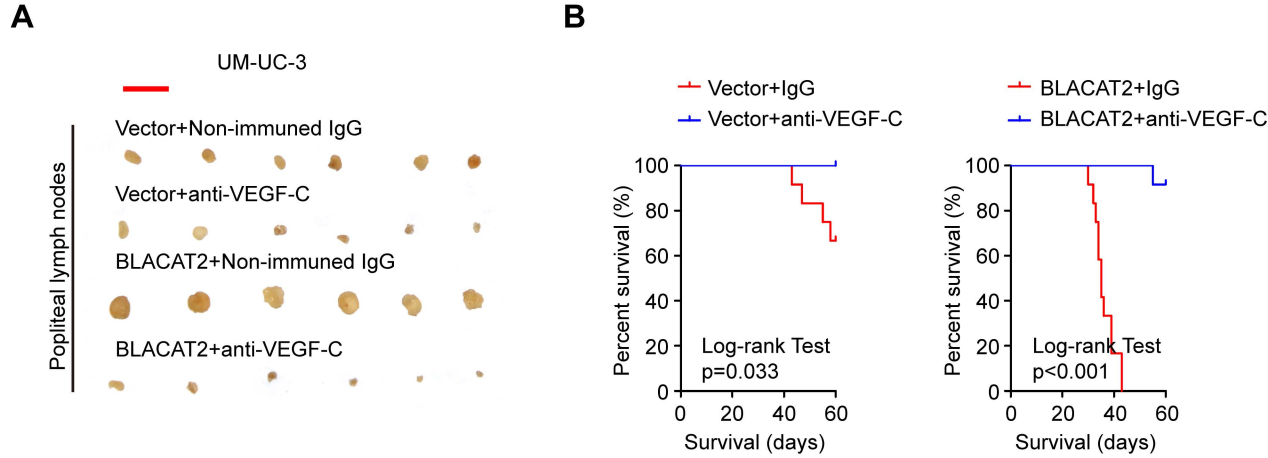

Supplemental Figure 27

Inhibition of VEGF-C abrogates BLACAT2-induced LN metastasis in vivo. (A) Representative images of popliteal LNs after VEGF-C ablation using a neutralizing antibody (n=12 per group). Scale bar: 5 mm. (B) Kaplan-Meier survival analysis of mice inoculated with the indicated cells.

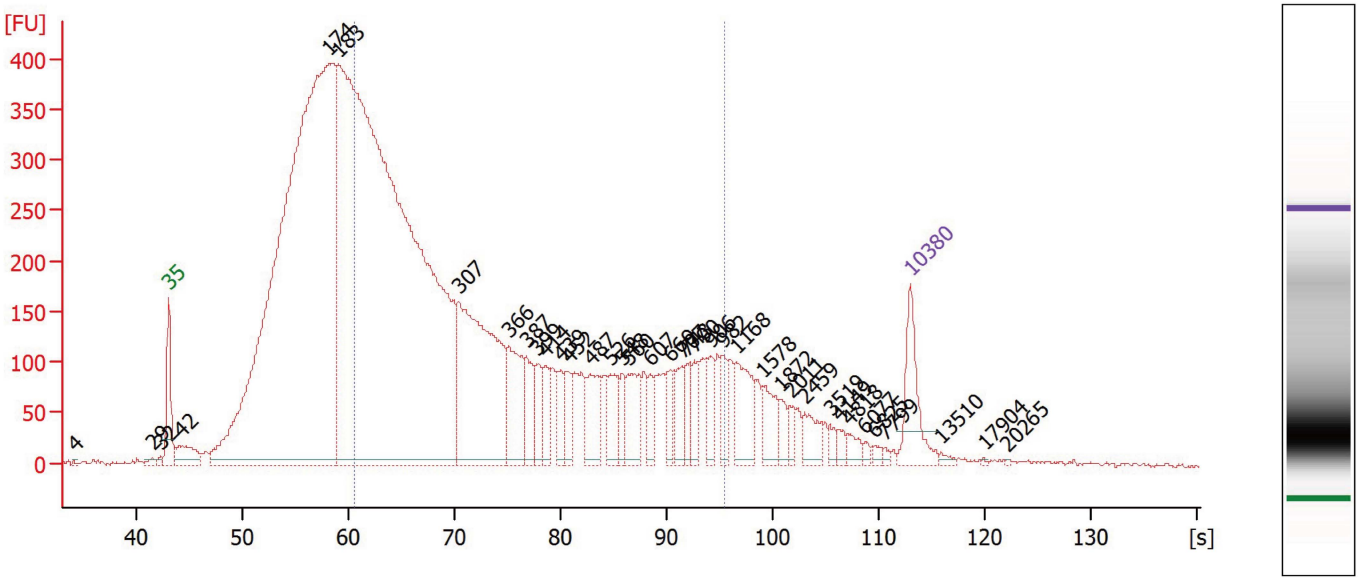

Supplemental Figure 25, for the editor and reviewers only
Representative image showing the distribution of sonicated DNA fragments determined by Agilent 2100.